

Evaluation of Constructed, Cast-in-Place (CIP) Piling Properties

Dr. Devin K. Harris, Dr. Theresa M. (Tess) Ahlborn, P.E.
Kevin Mears, Amir Gheitasi

Michigan Technological University
Department of Civil & Environmental Engineering

WisDOT ID no. 0092-09-04

December 2011

(This document is part 2 of 2 due to Web site file size limitations. For an electronic copy of the document in its entirety, contact research@dot.wi.gov.)



RESEARCH & LIBRARY UNIT



WISCONSIN HIGHWAY RESEARCH PROGRAM

WISCONSIN DOT
PUTTING RESEARCH TO WORK

4 Analysis

In this section the tests, outlined earlier, are analyzed and several are compared to the finite element model solutions for the stub-sections. This finite element model comparison includes variations in the concrete strength obtained from core testing, along with revised concrete strengths that take into consideration confinement. The results in this section include the concrete core samples, loading of the whole section, loading of the core section only, flexural testing, and the push-through testing. It should be noted that none of the stub sections were tested to failure because the load frame was unable to provide sufficient load to induce failure.

4.1 Concrete Core Samples

The concrete core samples were taken from the different locations along the length of the pile (Figure 13) and were tested in compression on the Baldwin frame (Figure 15). The cores were tested following the procedures of ASTM C31 (2003), however some variations were required due to some of the cores breaking shorter than required. The full results from all of the tests are listed in Appendix A, and the average compressive strengths are presented in (Table 6 and Figure 30). Some data points are missing because some of the cores broke during extraction and could not be tested as noted in Appendix B. This type of failure is not uncommon during coring operations and is a result of unexpected moments from the coring resulting in tensile failure of the cored concrete. This type of premature failure is not considered indicative of poor quality concrete as other specimens were extracted without occurrence. Also cores shorter than 7 in. were not used to calculate the averages. These average compressive strengths of the core samples are far greater than that of the test cylinders cast at the same time (7,600 psi vs. 4,700 psi).

Table 6 - Average Core Sample Compressive Strengths

Depth	10-3/4" dia. Piles (Pile 1,2)		12-3/4" dia. Piles (Pile 3, 4)	
	Compressive Strength (psi)	# of specimens	Compressive Strength (psi)	# of specimens
1-5 ft.	6,008	3		
5-10 ft.	8,218	4	7,378	7
10-15 ft.			6,509	4
15-20 ft.	9,119	3		
20-25 ft.	7,619	3		
25-30 ft.	7,875	3	6,545	1
30-35 ft.	7,754	3	7,073	4
35-40 ft.	9,427	2	8,195	3

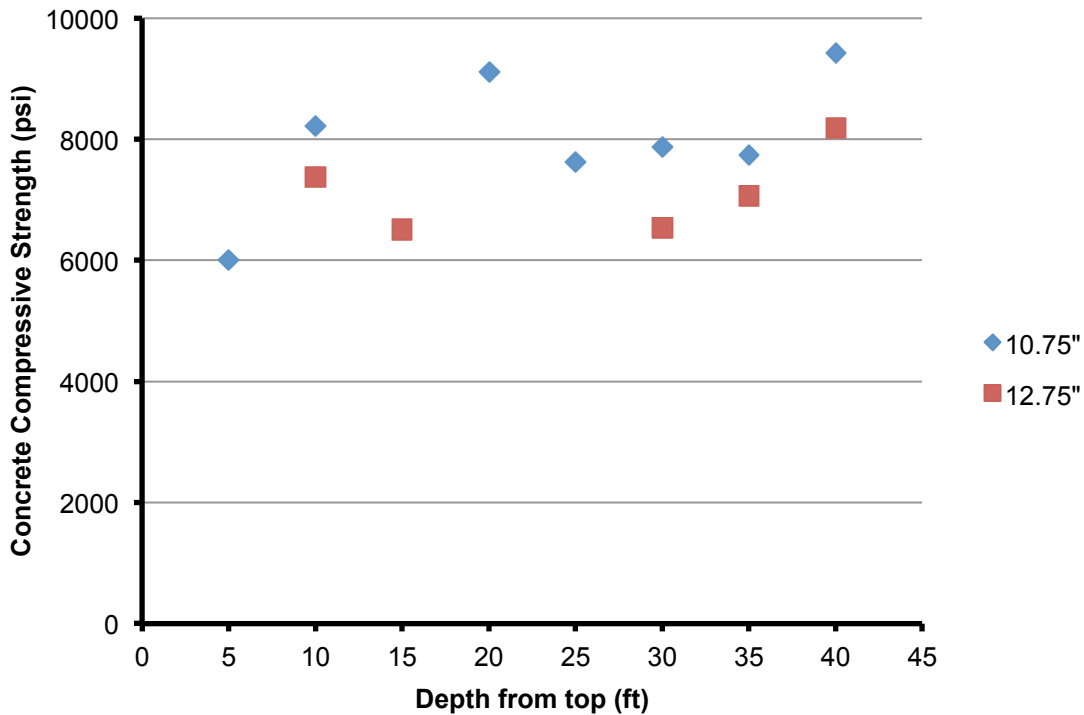


Figure 30 - Average Core Sample Compression Strengths through the depth

This increase in strength could be attributed to multiple factors. The water in the concrete in the piles may not have been able to escape, so a larger portion of the cement was hydrated, or the weight of the concrete pushing down in conjunction with the confinement from the steel shell could have densified the concrete, or the coring

process may have relieved some stress from the sections and helped align the crystalline structure of the cement by re-hydrating more cement to make it stronger.

The concept that the core concrete would have a lower strength was originally derived from the fact that the concrete was allowed to free-fall during placement and limited vibration was provided. These practices lead to the hypothesis that the concrete may be poorly consolidated or have some segregation that could not be accounted for in design. During the cutting phase of the project, the project team did not observe any significant defects at the ends of any member beyond that which would be expected from the cutting operations. In fact, the concrete consistently appeared to be well consolidated throughout based on visual observation.

4.2 Full Cross-Section Loading

Full cross-section testing was performed on a total of twelve stub-sections, four of each cross section size (Figure 13). In the numerical study, the compressive load was applied to the specimens using a thick steel plate between the loading jack and the pile stub-section, as it was actually performed for the experimental studies. This would generally represent a displacement - controlled problem. In this regards, specific attention was given to the loading configuration of the tubular piles in the finite element simulations, because the cross-section of the specimens was composed of two different materials with different modulus of elasticity. To have a uniform stress distribution and deflections all over the specimen, the external load applied was non-uniform distributed pressure on different parts of the cross section, with respect to the corresponding material properties. This would ensure the state of pure displacement-controlled conditions, which were fully considered in the corresponding numerical and experimental investigation. These material-dependent applied pressures on the stub sections can be calculated by satisfying the deflection compatibility and equilibrium conditions simultaneously, as given by Equation 11 and Equation 12.

$$\textit{Compatibility: } \sigma_s = n \times \sigma_c \quad \text{Equation 11}$$

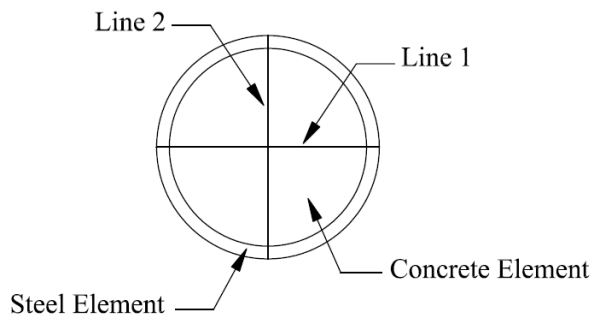
$$\textit{Equilibrium: } P_{MAX} = \sigma_s \times A_s + \sigma_c \times A_c \quad \text{Equation 12}$$

where A_s and A_c are the areas of steel and concrete portions in the cross section, σ_s and σ_c are applied uniform pressure on the steel and concrete portions, n is the ratio of steel to concrete modulus of elasticity, and P_{MAX} is the maximum applied load according to the limitation of the loading frame. As a result, the corresponding applied pressures with respect to the material properties and geometrical characteristics for all three types of piles and also compressive strength of the concrete core are summarized and given in Table 7.

Table 7 - FE composite loading for displacement controlled conditions

Pile No.	Cross section dimension	Material-dependent applied pressure (ksi)					
		f'_c : 4.50 ksi		f'_c : 5.85 ksi		f'_c : 8.00 ksi	
		σ_s	σ_c	σ_s	σ_c	σ_s	σ_c
Pile 1	10.75" dia. (0.375" wall)	44.289	5.840	41.615	6.256	38.416	6.754
Pile 2	10.75" dia. (0.500" wall)	38.543	5.08	3.597	5.502	4.215	6.015
Piles 3 & 4	12.75" dia. (0.375" wall)	33.08	4.471	31.665	4.760	29.017	5.101

The appropriate boundary conditions on the bottom side of the pile section were also applied as depicted in Figure 31. The proposed boundary conditions ensure the state of pure vertical compaction by neglecting the shear distortion due to Poisson's expansion/contraction effects. On the other hand, the axial load can be equally distributed along the cross section neglecting different material properties. In this case, the loading scenario would dictate the load - controlled conditions. The differences between two loading scenarios are illustrated in Figure 32 to shed light on this issue. The contour display in Figure 32 is presented to illustrate the relative effects of boundary conditions and symmetry on the pile response and as such the magnitudes are not included.

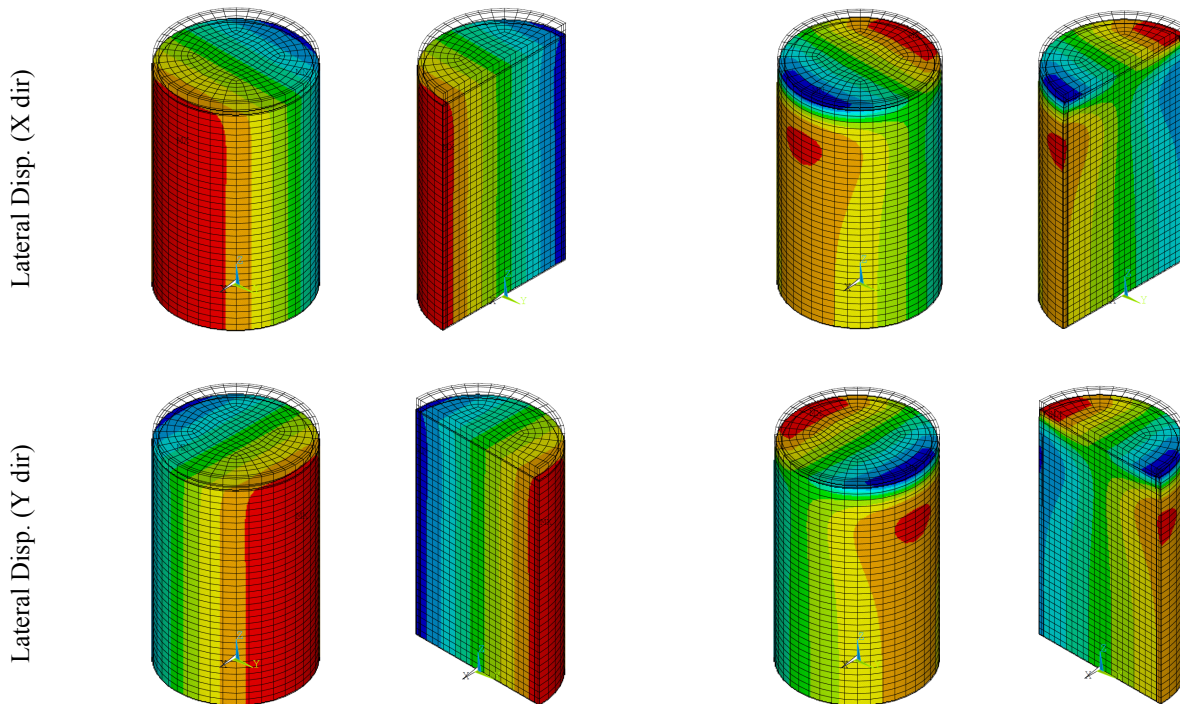


Boundary	U_x	U_y	U_z
Line 1	0	1	1
Line 2	1	0	1
Other nodes at $z = 0$	0	0	1
Free: 0	Fixed: 1		

Figure 31 - Applied boundary condition for full cross section loading scenario

(a) Proportionally Distributed Stress
"Displacement - Controlled"

(b) Uniformly Distributed Stress
"Load - Controlled"



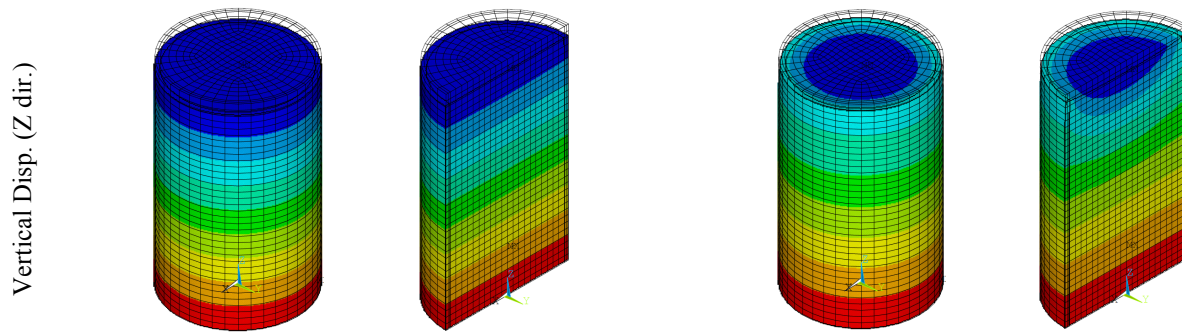


Figure 32 – Pile deformations (a) displacement-controlled (b) load-controlled

To monitor the response of the specimens under the applied loading, the load, and longitudinal and tangential strains at the mid-height of the sections were measured in both numerical and experimental studies. In order to have more logical and realistic interpretation, the applied load was converted to a longitudinal effective applied stress for a comparison of stress-strain response. To determine the equivalent applied stress on these samples, a transformed section analysis was performed converting the concrete to an equivalent steel section (see Equation 13).

$$A_{eff} = A_s + \frac{A_c}{n} \quad \text{Equation 13}$$

The steel material was chosen as the basic material in the cross section transformation, in view of the fact that the corresponding strains were recorded based on the data collected from the strain gauges attached to the external surface of the pile. The effective area based on the material properties and cross section dimensions are given in Table 8.

Table 8 - Effective cross sectional area

Pile No.	Cross section dimension	Effective cross section area (in ²)		
		f _c : 4.50 ksi	f _c : 5.85 ksi	f _c : 8.00 ksi
Pile 1	10.75" dia. (0.375" wall)	22.578	24.030	26.030
Pile 2	10.75" dia. (0.500" wall)	25.945	27.325	29.227

Piles 3 & 4	12.75" dia. (0.375" wall)	29.492	31.581	34.463
-------------	---------------------------	--------	--------	--------

For all pile specimens, the nominal capacities were calculated based on the composite as well as non-composite design methods (AASHTO 2010), and the corresponding results are presented in Table 9.

Table 9 - Nominal axial capacity used for design

Pile No.	Cross section dimension	Nominal capacity (kips)	
		Composite	Non-composite
Pile 1	10.75" dia. (0.375" wall)	972	240
Pile 2	10.75" dia. (0.500" wall)	1170	228
Piles 3 & 4	12.75" dia. (0.375" wall)	1234	346

For all specimens, the load was applied concentrically to a maximum level of 1000 kips, the capacity of the testing frame. The corresponding longitudinal and tangential strain distributions are depicted in Figure 33, derived from ANSYS as an output contour. Similar to the entire section loading scenario, the contour display in Figure 33 is presented to illustrate the relative effects of boundary conditions and symmetry on the pile response and as such the magnitudes are not included. Figure 34 - Figure 36 also illustrates the load vs. longitudinal strains as well as tangential strains for all specimens with different geometrical properties from both the experimental and numerical investigations. By converting applied loads into longitudinal stress using section transformation, the effective applied stresses vs. longitudinal and tangential strains are also depicted in Figure 37 - Figure 39 for a comparison of stress-strain response among different piles.

Strain Pile 1 Pile 2 Piles 3 & 4

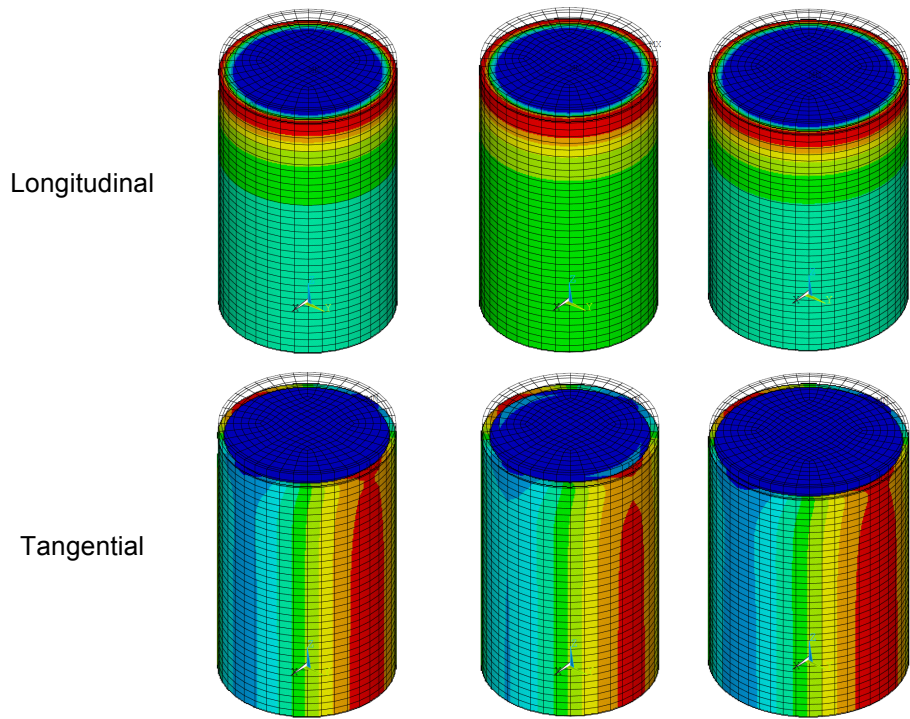


Figure 33 – Strain distribution contours (composite loading)

Pile 1 (10.75" dia. with 0.375" wall)

Pile 1 (10.75" dia. with 0.375" wall) specimens, exhibited the largest strains during the test, and demonstrated compatible results compared to the numerical analysis. From Figure 34 and Figure 37, it can be observed that most of the pile tests exhibited similar behavior, with the exception of pile section 1J (Run 1), which experienced larger longitudinal strains than the rest of the piles. This section was tested again (Pile 1J Run 2 and Run 3), and these other runs exhibited similar responses to the other cross-sections of the same size. Upon inspection of the specimen, it was found to have some irregularities on the top and bottom surfaces. This section had a small section of the steel shell and concrete core that was slightly elevated over the rest of the cross section, coincidentally directly above where the strain

gauge was located. This caused the strain gauge to be located on the face with greatest compressive stress during the initial test. After the first test, the surfaces were flattened out to where the cross section was uniformly loaded. This was found to be a reoccurring problem for several test sections. There were two samples (Pile 1D all runs and Pile 1J Runs 2 and 3) that approached yielding; however the frame was at capacity and more load could not be applied to cause yielding. Runs 2 and 3 for Pile 1J appear to have reached the yielding, but this cannot be verified as this was so close to the maximum load from the load frame that a change in slope is not evident. The tangential strains are much lower than the longitudinal strains because the load was applied along the longitudinal axis, and the resulting strains are only due to the radial expansion of the concrete and steel due to Poisson's effects. When comparing the effect of concrete compressive strength on transverse system behavior (e.g. Model 1 vs. Model 2), the impact is minimal. This is mostly attributed to the steel section being much stiffer (i.e. lower degree of radial expansion) than the concrete core.

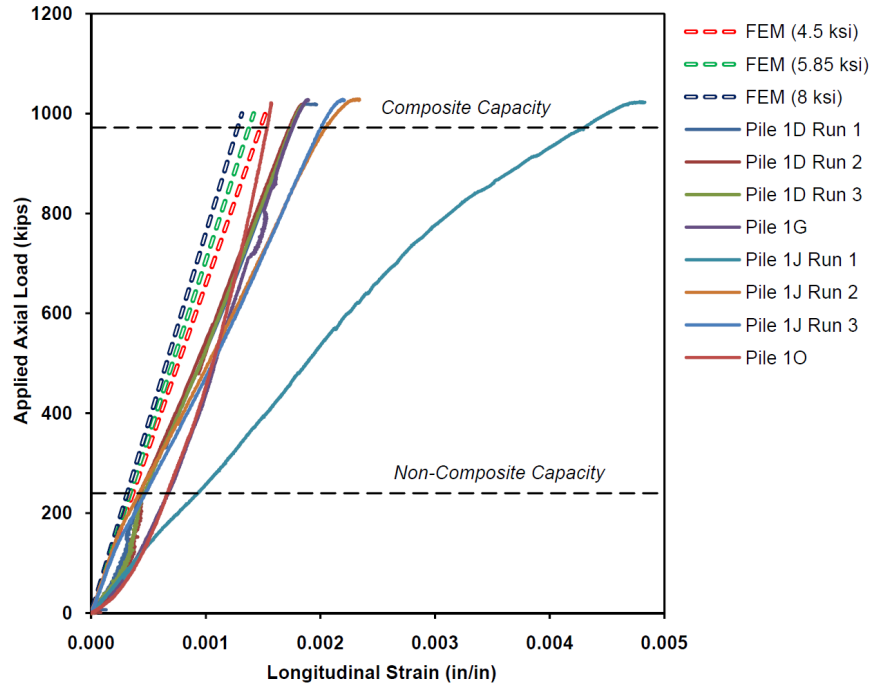
Pile 2 (10.75" dia. with 0.5" wall)

Pile 2 (10.75" dia. with 0.5" wall) specimens had the same outer diameter as the smallest cross section, but had a thicker steel wall. Due to the thicker shell, it was expected to have similar strengths to that of the 12-3/4 in. diameter specimens (Table 9), but with smaller strains than the Pile 1 sections. From Figure 35 and Figure 38, a common trend can be observed with pile sections 2H and 2S. Trials 2F and 2Y both had similar issues with the location of the strain gauges and a small section of the end surfaces not being perfectly flat as pile section 2H and 2S. Pile section 2F was found to have a small section of the steel shell and concrete core that was slightly higher than the rest of the cross section and this was located on the same side as the strain gauge. This caused the strain gauge to be at a location of greater pressure like section 1J of the 10-3/4" dia. (0.375" wall). Conversely pile section 2Y, had a spot that was higher than the rest, but the strain gauge was located on the opposite side of the high spot. This caused the strain gauge to experience very little compressive strain, until the high spot flattened out and then the strains started to increase with the load. Pile section 2H

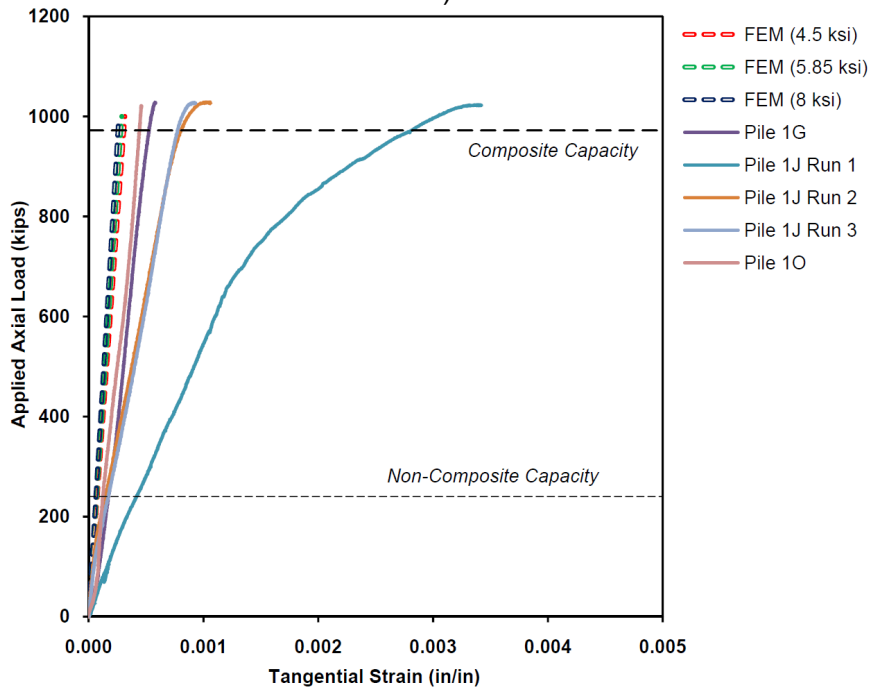
has a load unload loop in the data, as there was a small section of elevated concrete on the surfaces when the loading occurred. This small section was loaded until it began to crack at which the load increased at a quicker rate. After this concrete crushed and the head was loading the entire surface again it loaded back up until the maximum of the load frame. When comparing the load/stress – tangential strain relationships, it can be seen that three of the four tests were in relatively good agreement. Pile section 2F had a much larger tangential strain than the rest, as was the case for the longitudinal strains. These large tangential strains were caused by the same problem as the longitudinal strains, which occurred due to the strain gauge being located at a location with a deformity on the top surface, causing the location to be loaded more heavily. Similar to the pile 1 sections, the variation in concrete strengths did not affect the overall stiffness enough to influence the strains appreciably.

Piles 3 & 4 (12.75" dia. with 0.375" wall)

Piles 3 & 4 (12.75" dia. with 0.375" wall) specimens had the overall largest cross section of all specimens tested, and was predicted to have the greatest capacity; however, the 12.75 in. diameter samples did not exhibit similar behavior to the smaller specimens. These samples exhibited almost no strains in either the longitudinal or tangential directions from the testing (Figure 36 and Figure 39). It should be noted that the shell on the 12-3/4 in. diameter specimens was spiral welded as opposed to the two 10-3/4 in. diameter piles, which were seam welded. This spiral appears to have changed the way load was transferred throughout the section and, as such, the model was not able to simulate the true strains experienced by the sections. There was one 12-3/4 in. section where the strain gauges did record a much higher value than the rest of the 12-3/4 in. sections; however, in this test the strain gauge happened to be above the seam and also in a location where the top surface had a high spot. Because the spiral welded shell changes the way the load is transferred through the member it can be concluded that the developed FE model can accurately predict the strains of a stub section that is uniformly loaded and seam welded, however it should not be used with a spiral weld.

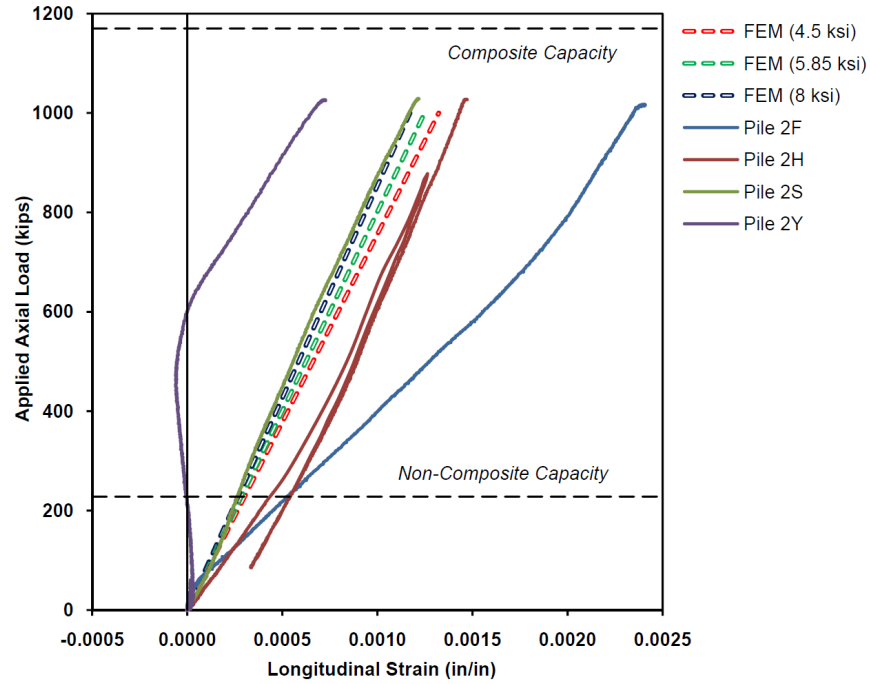


a)

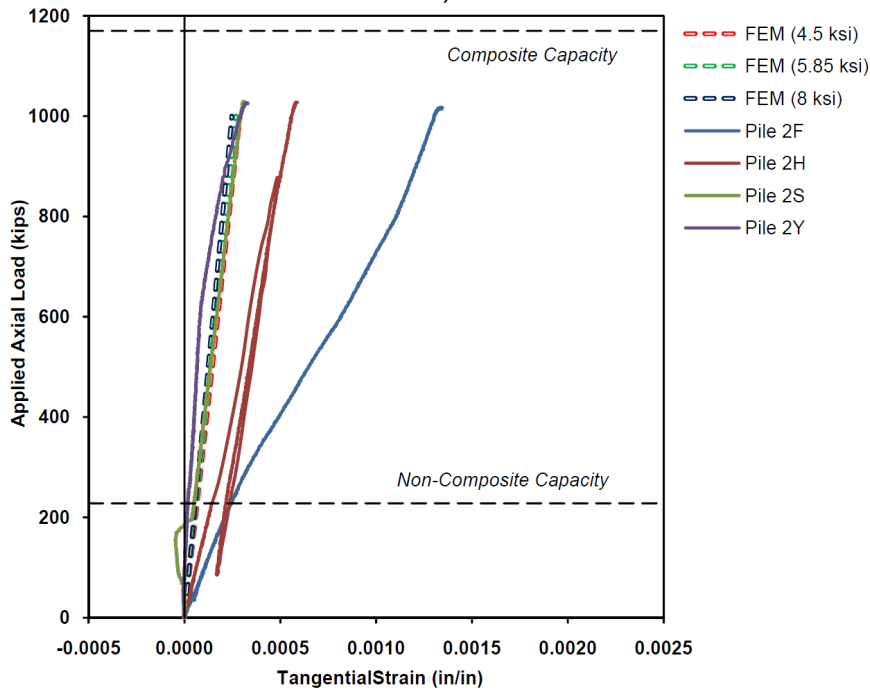


b)

Figure 34 - Pile 1 (10.75" - 0.375" wall) Load (composite) vs. a) longitudinal strain, b) tangential strain

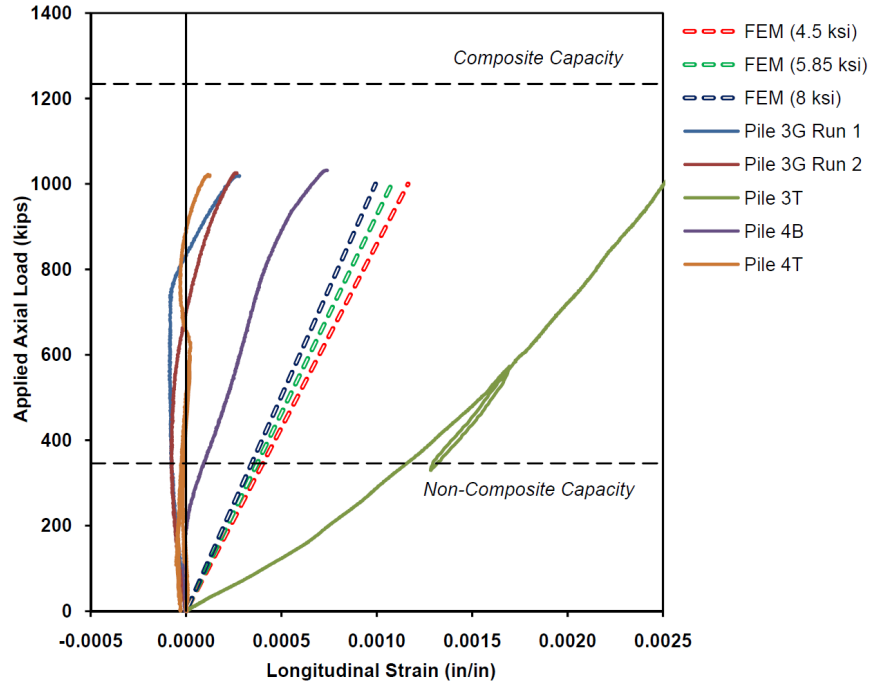


a)

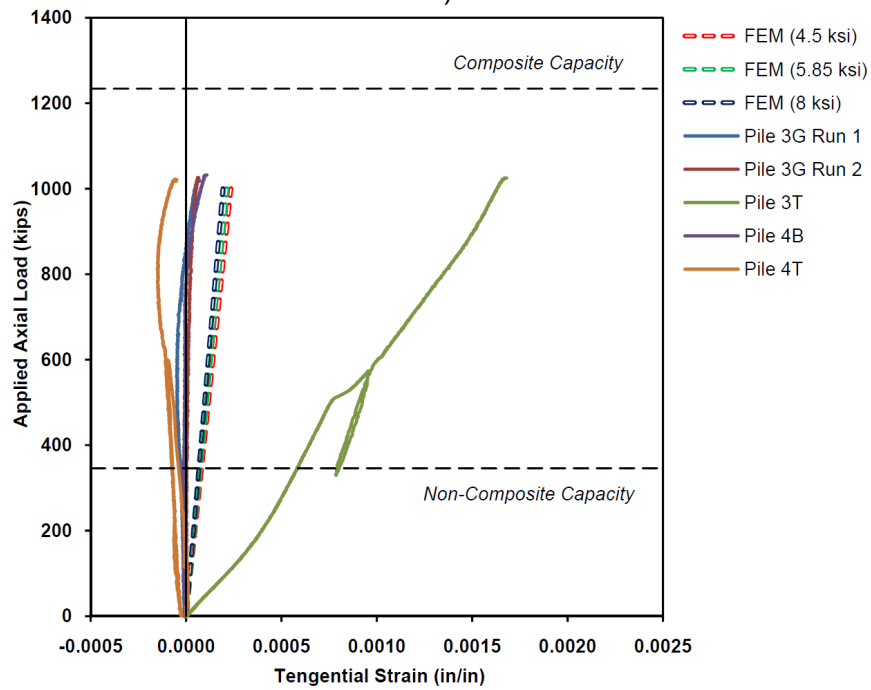


b)

Figure 35 - Pile 2 (10.75" - 0.5" wall) Load (composite) vs. a) longitudinal strain, b) tangential strain

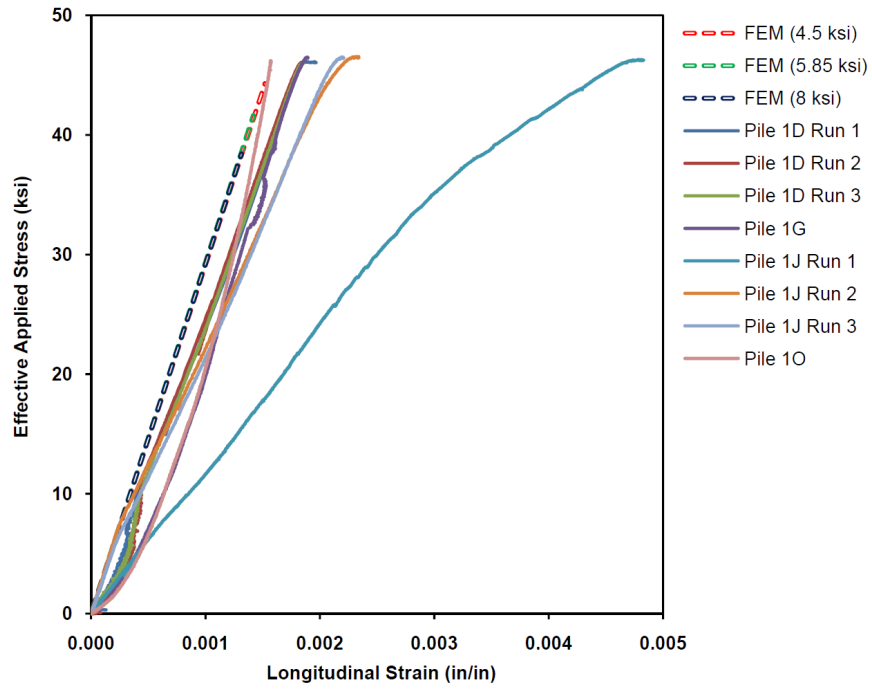


a)

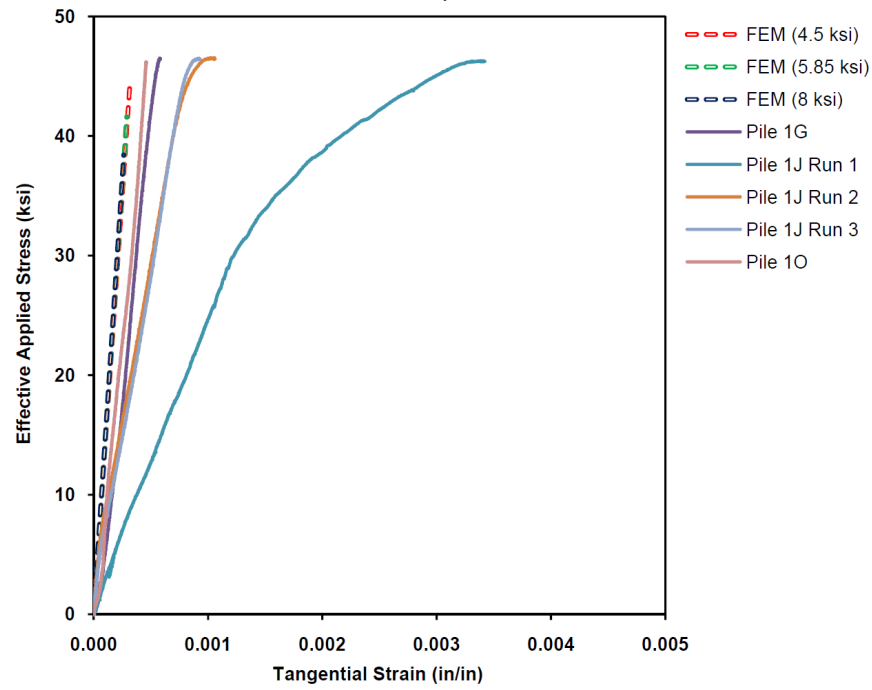


b)

Figure 36 – Piles 3 & 4 (12.75" - 0.375" wall) Load (composite) vs. a) longitudinal strain, b) tangential strain

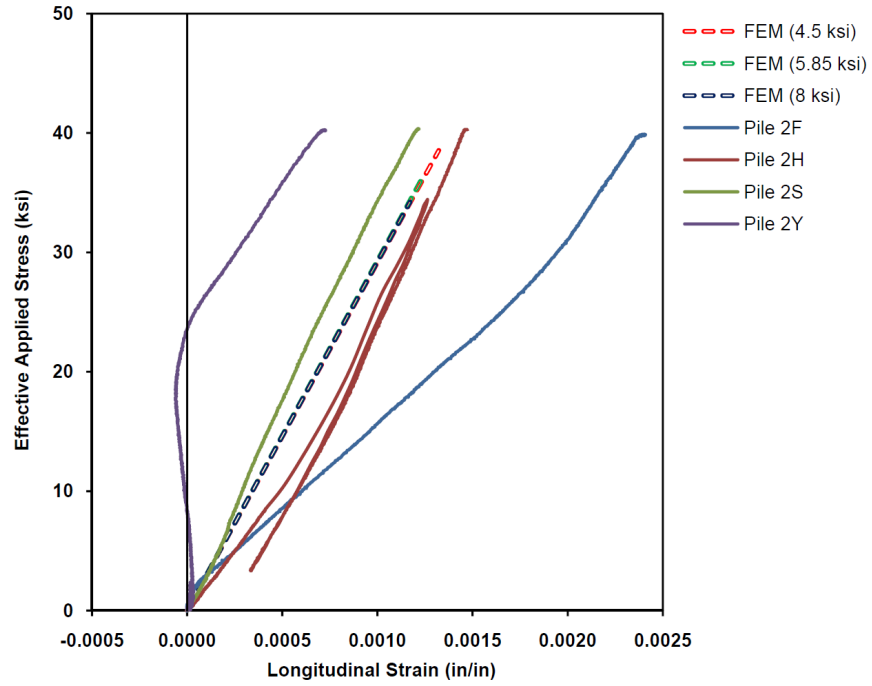


a)

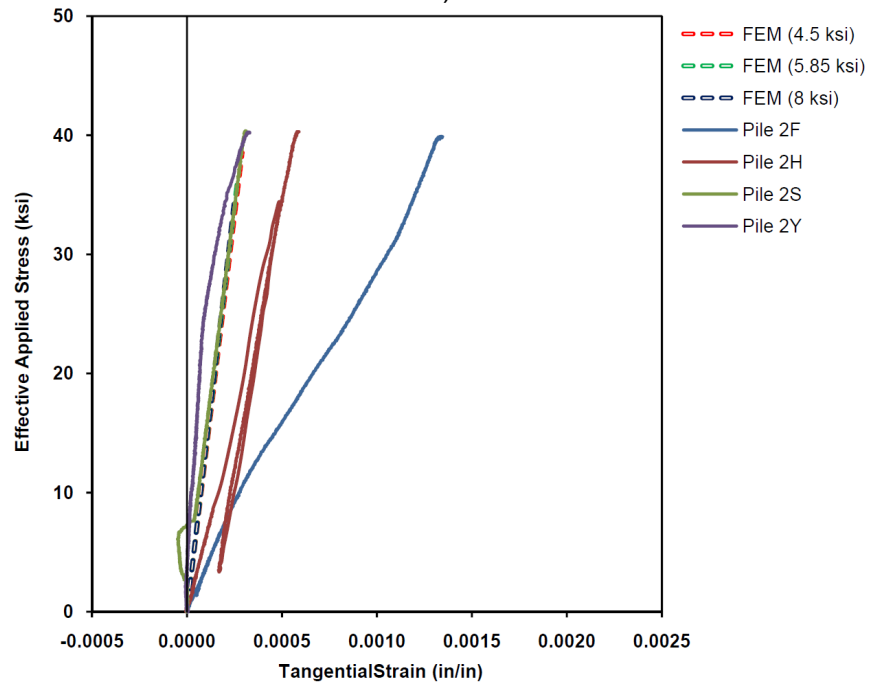


b)

Figure 37 - Pile 1 (10.75" - 0.375" wall) Effective stress (composite) vs. a) longitudinal strain, b) tangential strain

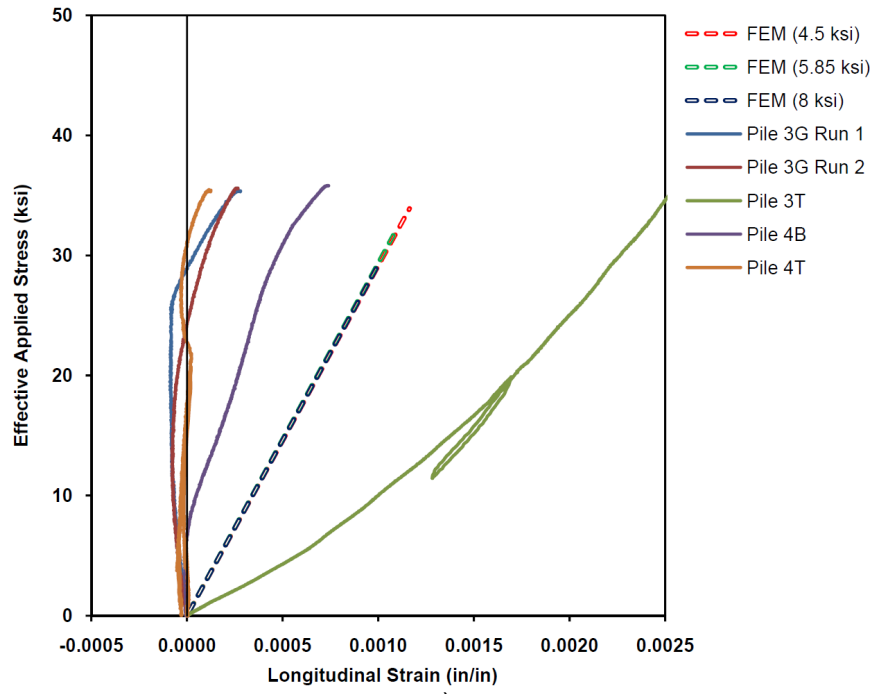


a)

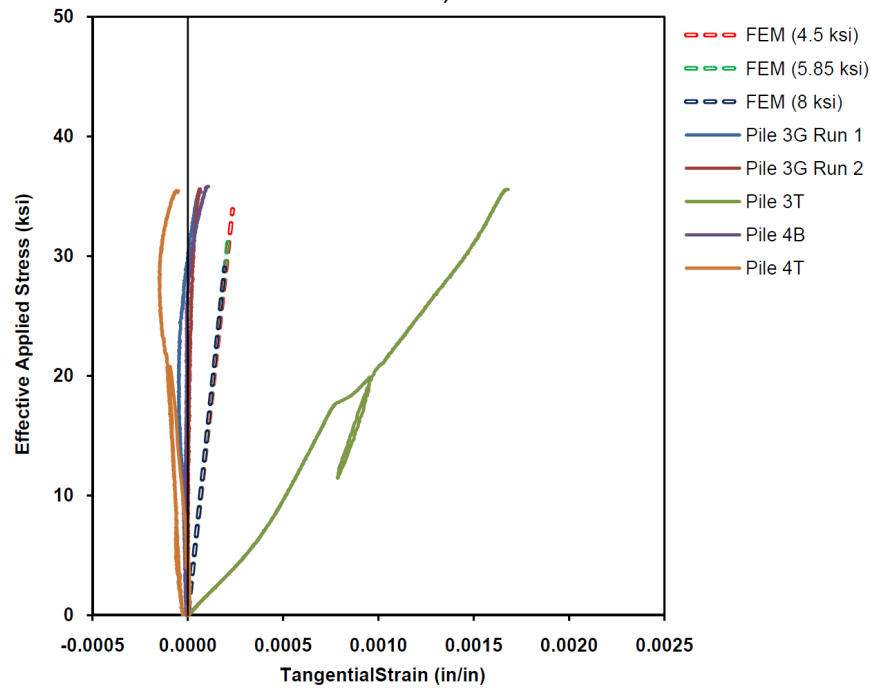


b)

Figure 38 - Pile 2 (10.75" - 0.5" wall) Effective stress (composite) vs. a) longitudinal strain, b) tangential strain



a)



b)

Figure 39 - Piles 3 & 4 (12.75" - 0.375" wall) Effective stress (composite) vs. a) longitudinal strain, b) tangential strain

4.2.1 Summary of Full Cross-Section Loading

Due to the increased wall thickness of the specimens used in the full cross-section loading scenario and the limitations of the testing frame, none of the specimens were tested to ultimate capacity. However, all specimens were tested to the limits of the testing frame (1,000 kips) without experiencing failure. For the piles, this load represents a 317%, 339%, and 189% increase over the non-composite nominal capacities on the 10-3/4" dia. (0.375" wall), 10-3/4" dia. (0.5" wall), and 12-3/4" dia. (0.375" wall), respectively. While this limitation was less than the composite section design capacity for all specimens except the 10-3/4" dia. (0.375" wall), all specimens remained in the elastic range at this upper bound loading. In addition, all of the loads on the specimens surpassed the nominal design capacity for the non-composite analysis without failure. While this finding is not a direct measure of the ultimate capacity, the performance of these piles indicates a significant amount of reserve capacity when considering the current design approach used in Wisconsin.

4.3 Section Core Only Loading

Compression testing of the stub section by loading only the core area was performed on the total of 12 different stub-sections, four for each cross section size. Unlike the previous test where the whole stub section was loaded, only the concrete core was loaded using a thick steel plate on both sides between the loading head and the pile stub sections. This would similarly represent a displacement-controlled problem. Although the section does have two different materials, the loading was applied to the concrete core. Therefore, the applied stress, σ_c , can easily be calculated solely based on the dimension of the core section, independent of the material properties, as given by Equation 14.

$$\sigma_c = \frac{P_{MAX}}{A_c} \quad \text{Equation 14}$$

where A_c is the area of the concrete core in the cross section, σ_c is the applied uniform pressure on the concrete core, and P_{MAX} is the maximum applied load according to the limitation of the loading frame. In essence, the corresponding applied pressures on the

central core, irrespective of the material properties and compressive strength of the concrete core, for all three types of piles are summarized and given in Table 10.

Table 10 - FE non-composite loading

Pile No.	Cross section dimension	Material-independent applied pressure (ksi)
Pile 1	10.75" dia. (0.375" wall)	σ_c : 12.732
Pile 2	10.75" dia. (0.500" wall)	σ_c : 13.394
Piles 3 & 4	12.75" dia. (0.375" wall)	σ_c : 8.842

For the boundary conditions, the same restraint scenario (Figure 31) from the composite loading scenario is applied on the bottom side of the pile stub sections, with the exception for the nodes corresponding to the steel external shell. In this case, the uniform pressure applies only on the concrete core. Thus, the support conditions also apply only on the central core because the specimen must undergo the same loading conditions on both sides, identical to the test setup. A representation of the differences in response between two applied boundary conditions (with and without neglecting the steel shell in applying the restraint) is illustrated in Figure 40.

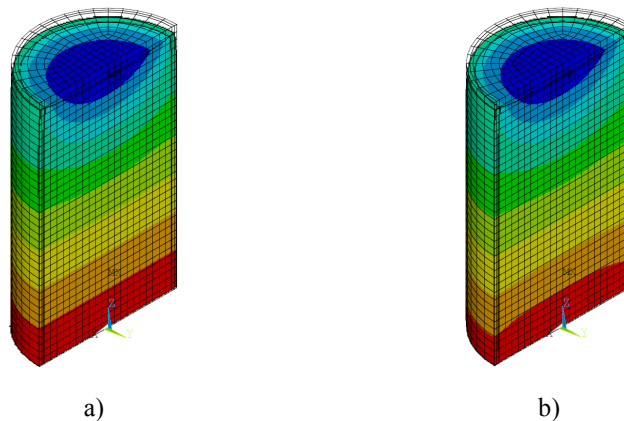


Figure 40 – Effect of applied boundary conditions a) composite section vs. b) core-only loading

Similar to the previous case, to monitor the response of the specimens under the applied loading condition, the load, longitudinal and tangential strain at the mid-height of the sections were measured in both numerical and experimental studies. Moreover, the applied load was converted to the longitudinal effective applied stress for comparison of stress-strain responses between the two corresponding loading scenarios. To

determine the equivalent applied stress on these samples, a transformed section analysis was performed converting the concrete to an equivalent steel section (Equation 13). Again, the steel material was chosen as the basic material in the cross section transformation, in view of the fact that the corresponding strains were recorded based on the data collected from the strain gages attached to the external surface of the pile.

The effective area based on the material properties and cross section dimensions were the same as given in Table 8. Furthermore, the nominal capacities of the piles are independent of the loading scenarios, and given in Table 4. For all of the specimens, the load was applied concentrically to a maximum level of 1000 kips, the capacity of the testing frame. The corresponding longitudinal and tangential strain distributions are depicted in Figure 41, derived from ANSYS as an output contour. Figure 42 - Figure 44 illustrates the load vs. longitudinal strains as well as tangential strains for all specimens with different geometrical properties for both the experimental and numerical investigations. By converting applied loads into longitudinal stress using section transformation, the effective applied stress vs. longitudinal and tangential strains are also depicted in Figure 45 - Figure 47. From the testing of the sections under the core loading, definite trends were observed.

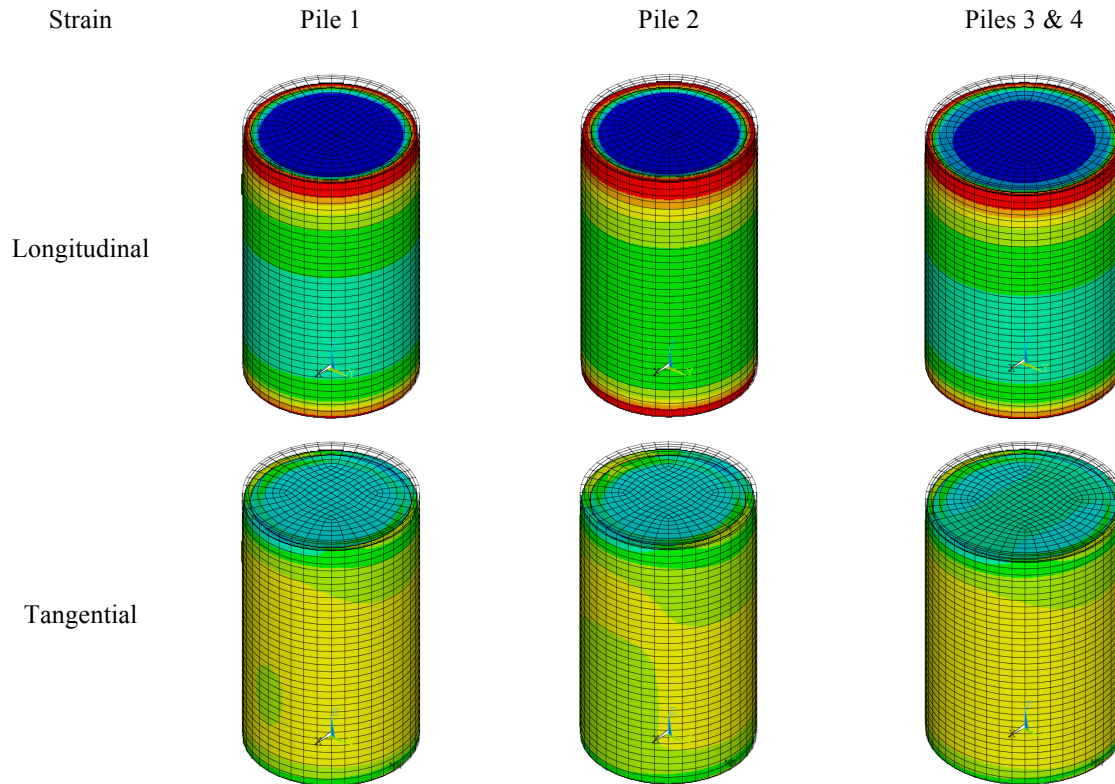


Figure 41 - Strain distribution contours (non-composite loading)

Pile 1 (10.75" dia. with 0.375" wall)

Pile 1 (10.75" dia. with 0.375" wall) specimens exhibited a significant variance from specimen to specimen for the longitudinal response, but parity in the tangential response. Pile section 1C had a region of the cross section surface that was slightly elevated and the strain gauge recorded strains around zero until the elevated section was leveled out during loading, at which point the whole section was simultaneously loaded. Overall the specimens experienced lower longitudinal strains than the equivalent composite loaded specimen as a result of the internal load transfer mechanism for this loading scenario. In this scenario, the load is applied directly to the core section and then redistributed (internal to the cross-section) to the steel shell via bond and expansion, resulting in a lower overall shell stress than the composite loading scenario. On the contrary, all four trials showed very similar tangential strains in the steel shell, which are generally higher than those observed from the scenario where the entire cross section was loaded. This is because the steel shell was not loaded in this

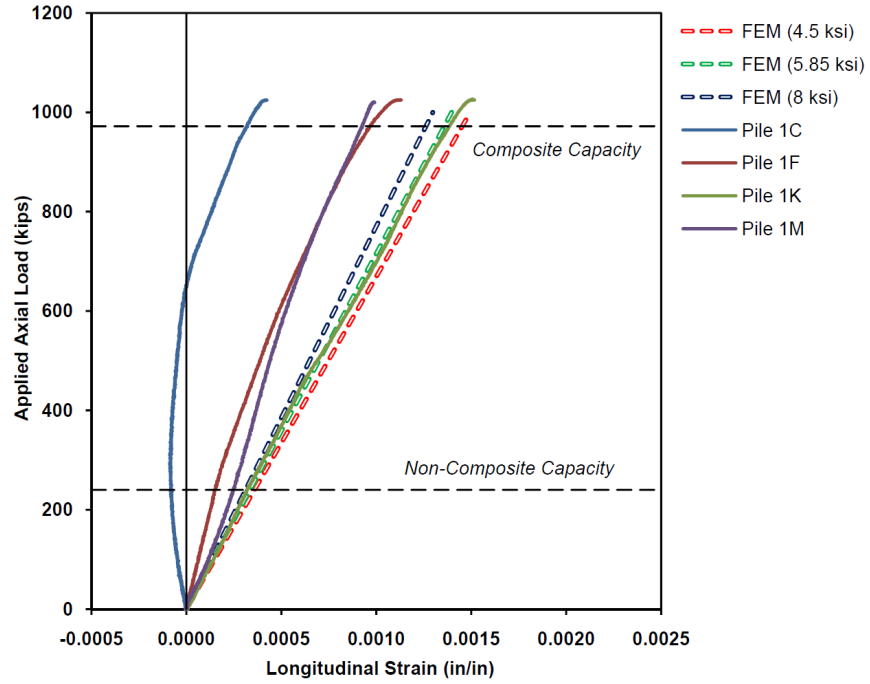
test and, as such, the concrete core is resisting more axial load and due to Poisson's effect pushing out in the radial direction, which induces strains in the steel in the radial direction.

Pile 2 (10.75" dia. with 0.5" wall)

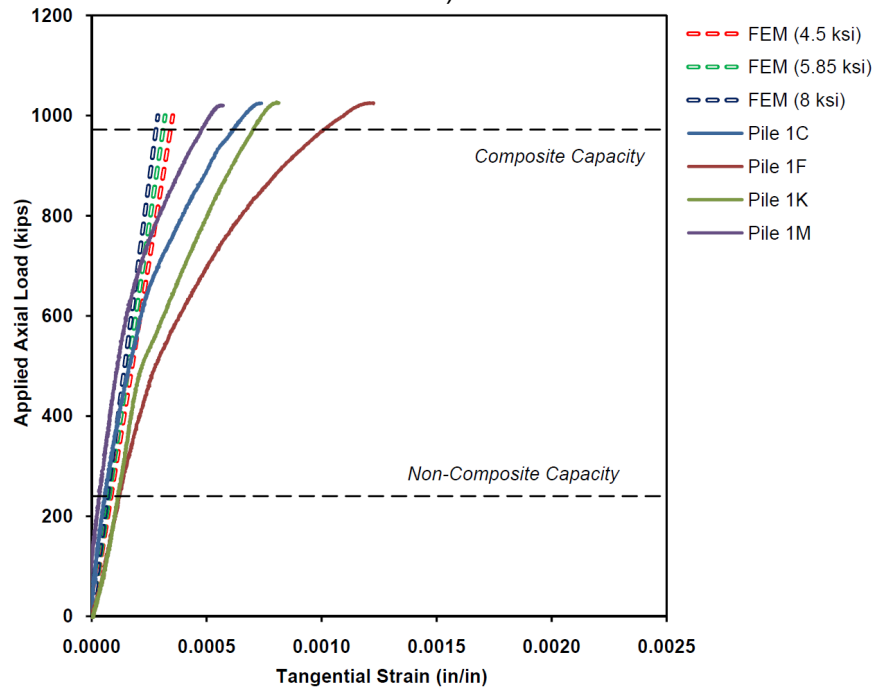
Pile 2 (10.75" dia. with 0.5" wall) specimens exhibited smaller longitudinal and tangential strains than the thinner (0.375") walled specimens as expected, but the response in both directions was similar to each other in magnitude. This was different from the loading of the whole section, where the tangential strains were much smaller than the longitudinal one. This is mostly caused by the steel shell only being loaded by the frame. Pile section 2I, had a high spot where the strain gauge was located, which caused the gauge to experience more strain at that location; however the other three runs all show very good agreement with each other under core loading. Similar to the Pile 1 specimens, the strains observed in the tangential direction, resulting from greater radial expansion, were higher for this loading scenario than the full composite section loading scenario.

Piles 3 & 4 (12.75" dia. with 0.375" wall)

Piles 3 & 4 (12.75" dia. with 0.375" wall) specimens for this loading case did not show a similar trend to the composite section loading scenario. For the loading of the core only, the spiral weld did not appear to affect the way the load is transferred through the section and a generally proportional increase in load with strain was observed for all specimens. However, contrary to the composite section loading scenario, the finite element model was able to better simulate both the longitudinal or tangential strains for the core only loading scenario, even in the presence of the spiral weld.

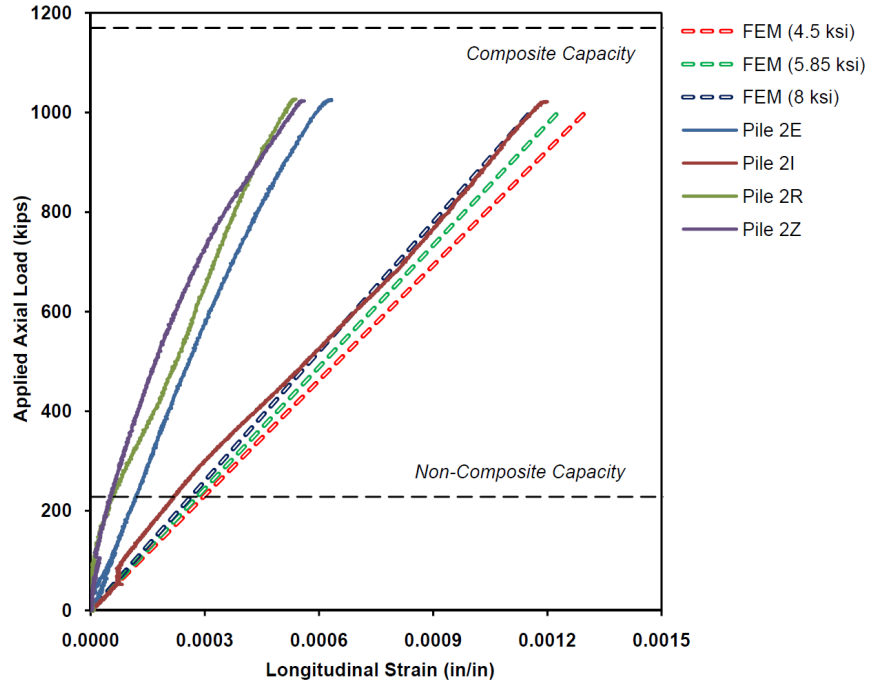


a)

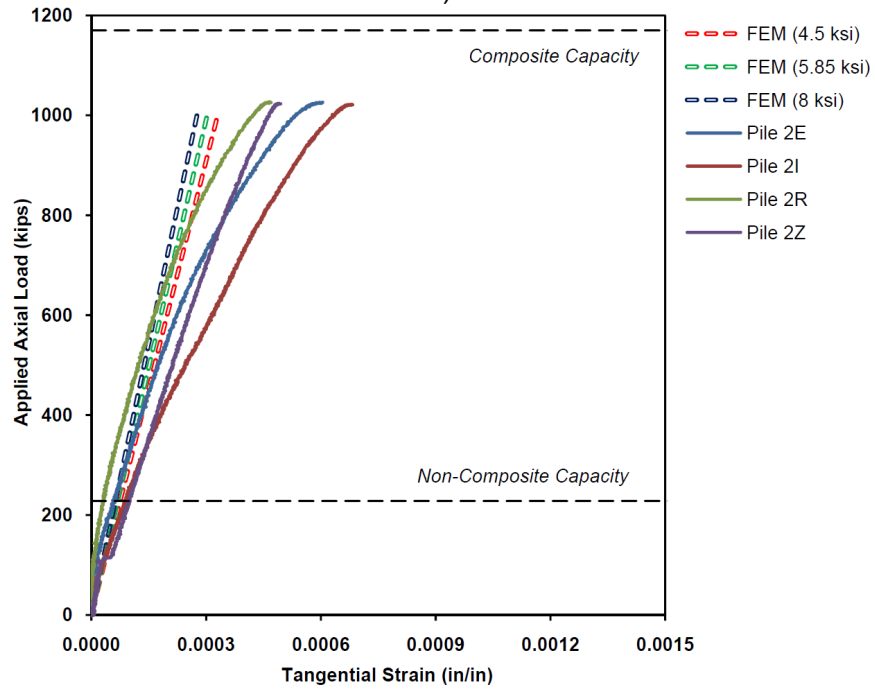


b)

Figure 42 - Pile 1 (10.75" - 0.375" wall) Load (core) vs. a) longitudinal strain, b) tangential strain

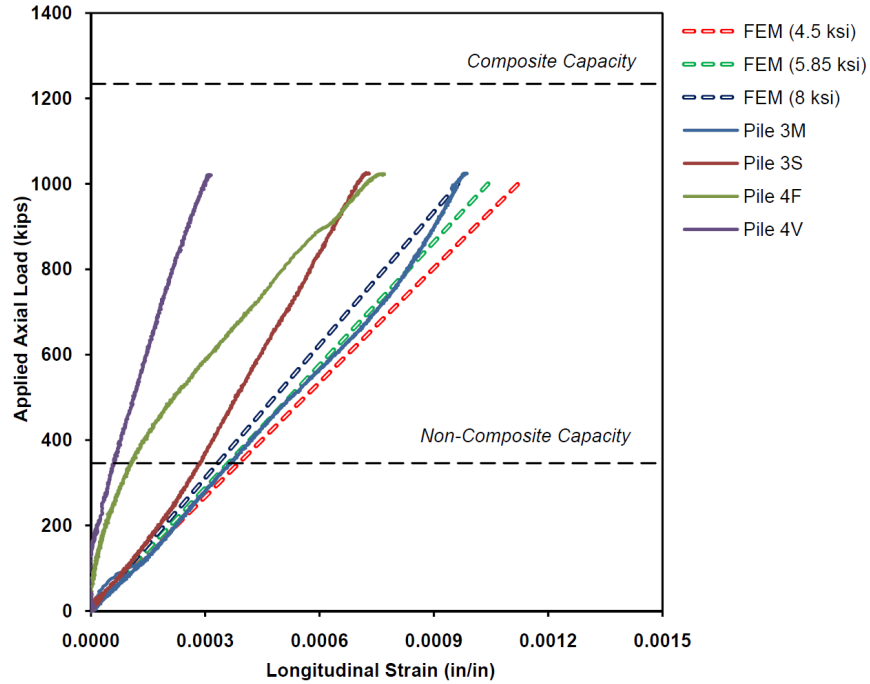


a)

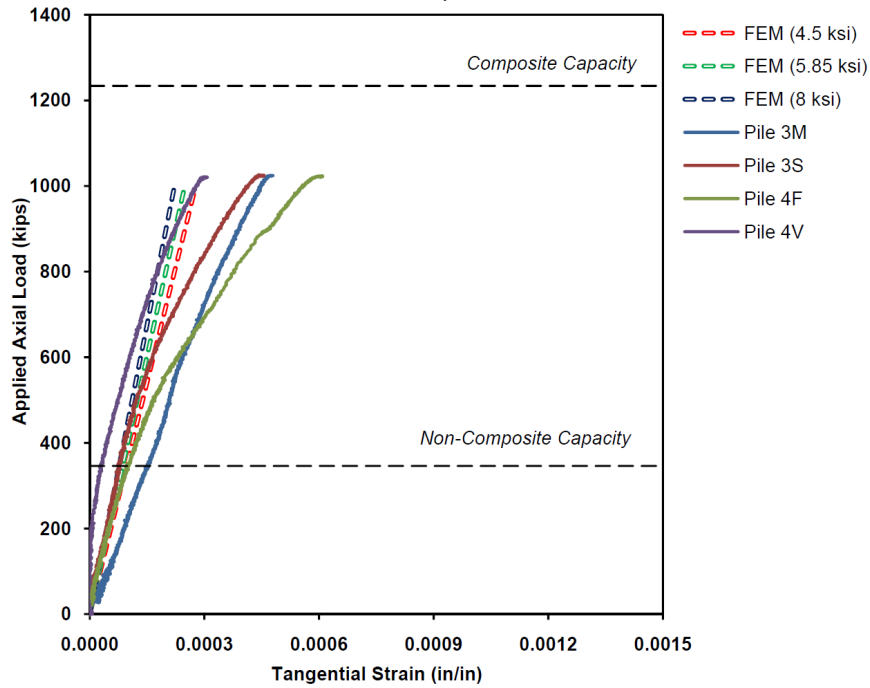


b)

Figure 43 - Pile 2 (10.75" - 0.5" wall) Load (core) vs. a) longitudinal strain, b) tangential strain

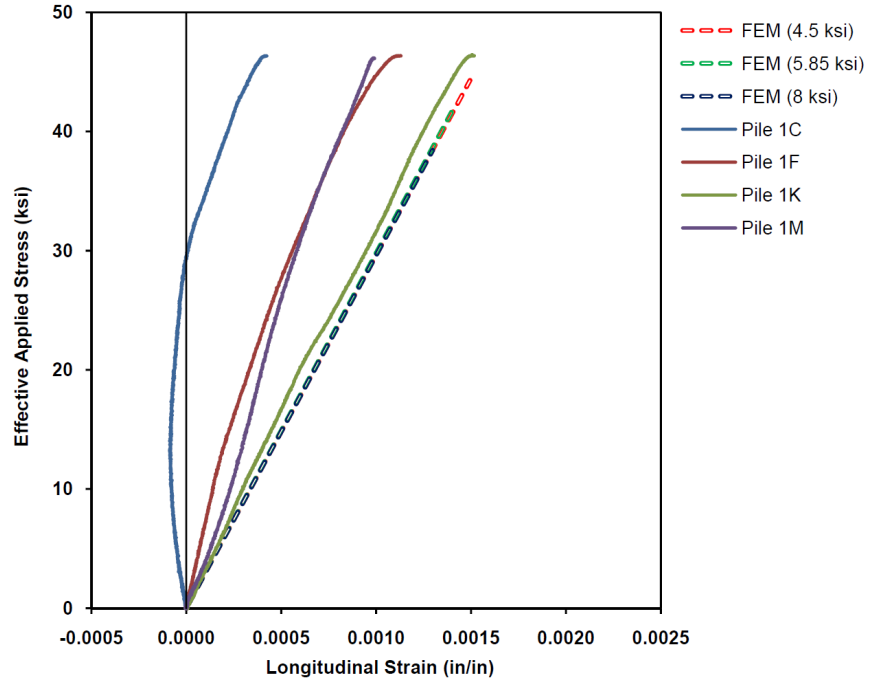


a)

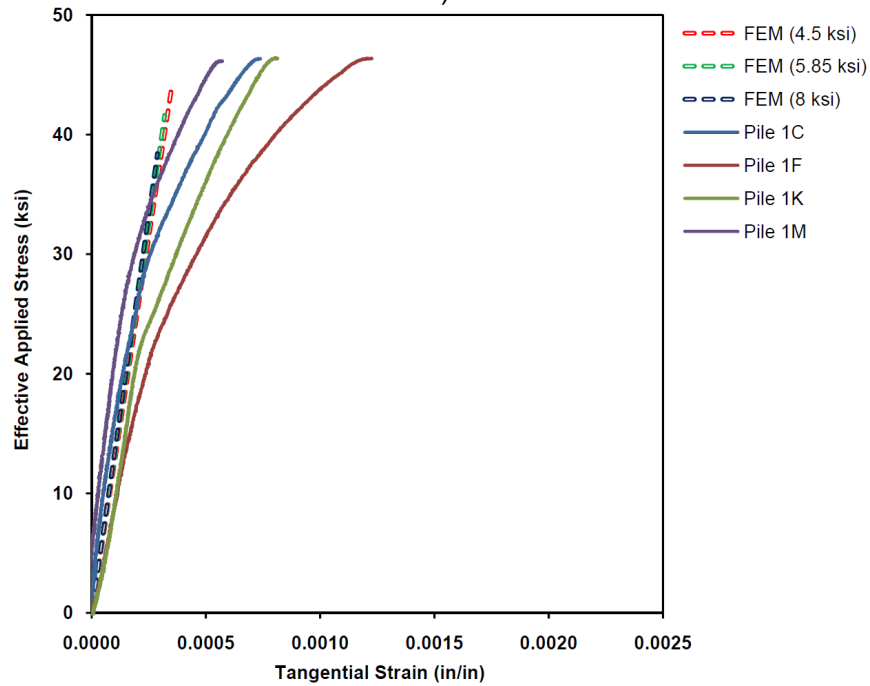


b)

Figure 44 – Piles 3 & 4 (12.75" - 0.375" wall) Load (core) vs. a) longitudinal strain, b) tangential strain

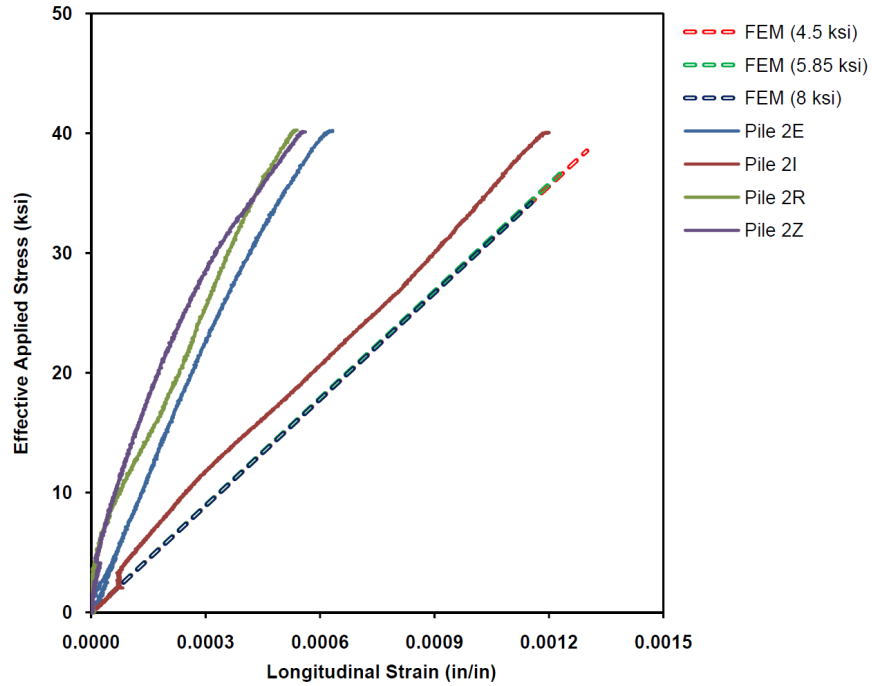


a)

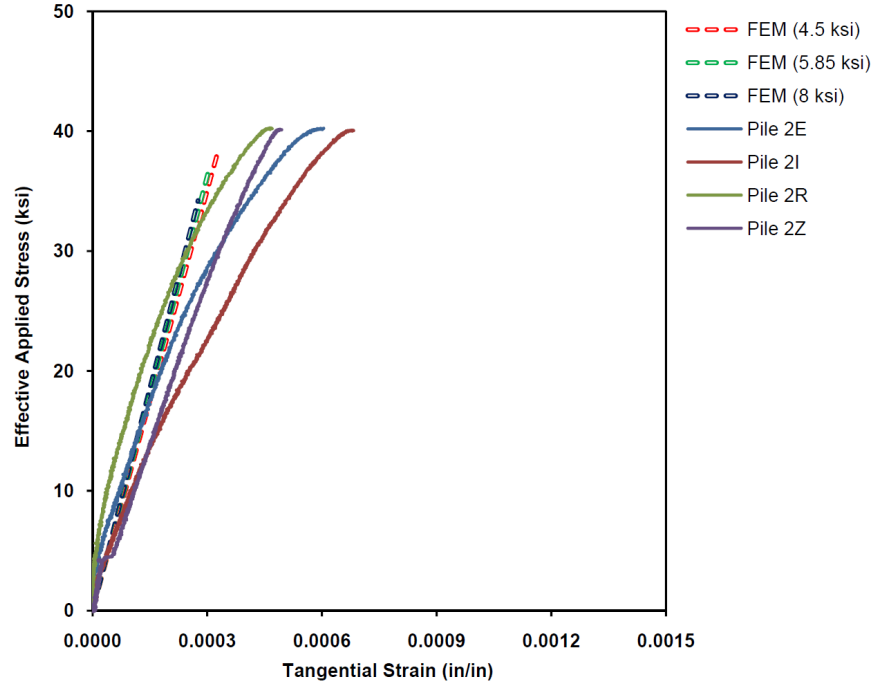


b)

Figure 45 - Pile 1 (10.75" - 0.375" wall) Effective stress (core) vs. a) longitudinal strain, b) tangential strain

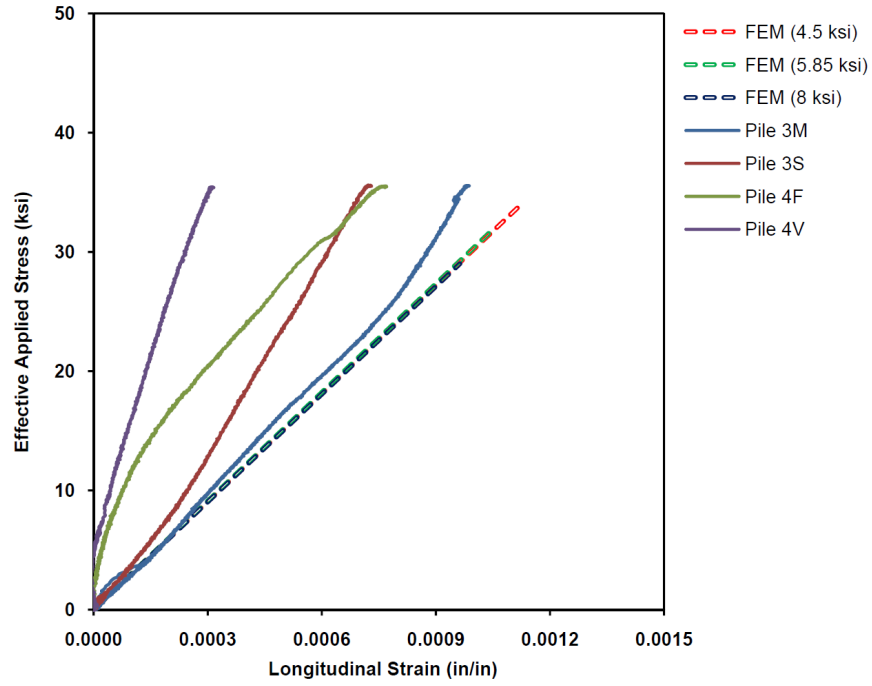


a)

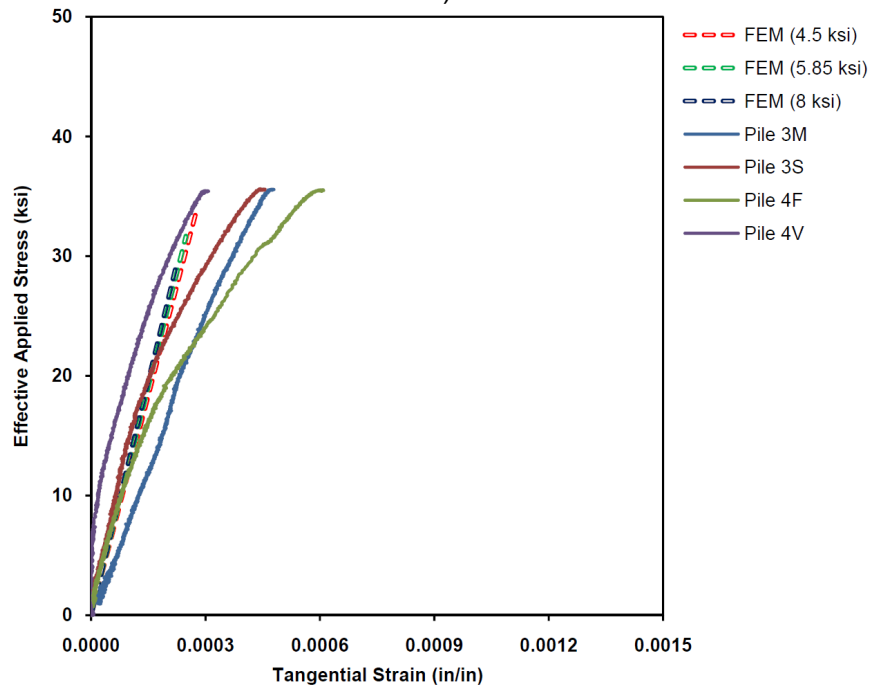


b)

Figure 46 - Pile 2 (10.75" - 0.5" wall) Effective stress (core) vs. a) longitudinal strain, b) tangential strain



a)



b)

Figure 47 - Piles 3 & 4 (12.75" - 0.375" wall) Effective stress (core) vs. a) longitudinal strain, b) tangential strain

4.3.1 Summary of Core Only Loading

Similar to the composite-section loading scenario, because of the increased wall thickness of the specimens used in the full cross-section loading scenario and the limitation of the testing frame, none of the specimens were tested to ultimate capacity. However, all specimens were tested to the limits of the testing frame (1,000 kips) without experiencing failure. Similar to the composite section loading scenario, this load represents a 317%, 339%, and 189% increase over the non-composite nominal capacities on the 10-3/4" dia. (0.375" wall), 10-3/4" dia. (0.5" wall), and 12-3/4" dia. (0.375" wall), respectively. While this limitation, was less than the composite section design capacity for all specimens except the 10-3/4" dia. (0.375" wall), all specimens remained in the elastic range at this upper bound loading. In addition, all of the specimens exceed the nominal design capacity for the non-composite analysis without failure. While this finding is not a direct measure of the ultimate capacity, the performance of these piles indicates a significant amount of reserve capacity when considering the current design approach used in Wisconsin.

4.4 Soil - Pile Interaction

As illustrated in Figure 48, the State of Wisconsin's soil series are grouped into fifteen general regions. In general the governing types of the soil in the state can be simply categorized as sandy, silty and loamy soils, which create the surface layers of the soil body above the bedrock.

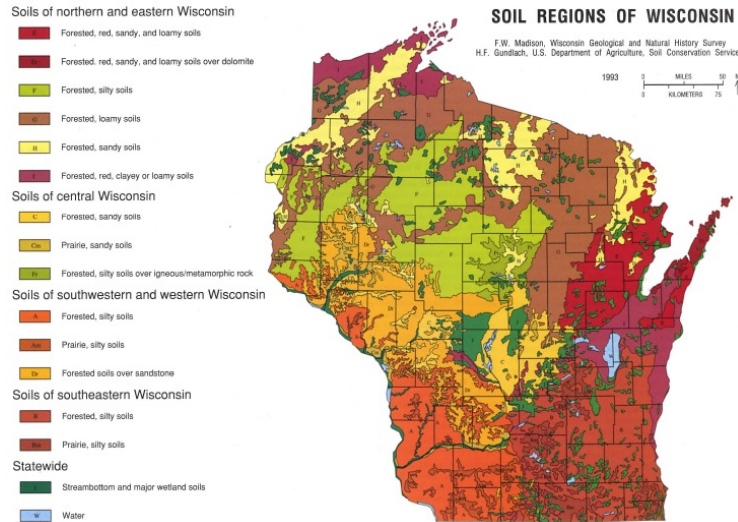


Figure 48 - Soil regions in the State of Wisconsin (Wisconsin Geological and Natural History Survey 2011)

While the thickness of unconsolidated soil is highly variable throughout the state, a large portion of the state has a thickness of approximately 50 ft. or less (Figure 49). In this study, it was assumed that the investigated piles most likely reached their limit in drivability due to side friction, which can be considered a reasonable assumption when comparing typical pile lengths (~40 ft.) to the thickness of the unconsolidated soil layer for most regions of the state. However, it should be noted that there was no attempt to correlate the thickness of unconsolidated soil with pile installation locations and this exercise was intended to be illustrative of the behavior of embedded piles only.

Based on the results obtained via numerical and experimental investigations, the piles themselves behave elastically under an applied load of a million pounds, provided that the bearing capacity of the bedrock is infinite. However, the bearing of the soil beneath the pile usually dictates the total capacity of the deep foundation system. As illustrated in Figure 50, dolomite, sand stone, and granite create the main fraction of the bedrock composition within the State of Wisconsin. Based on the WisDOT bridge manual (WisDOT 2011), a pile foundation transfers load into the underlying strata by either shaft resistance (R_S), point resistance (R_P) or a combination of both. Most of the driven piles develop some amount of both shaft and point resistance.

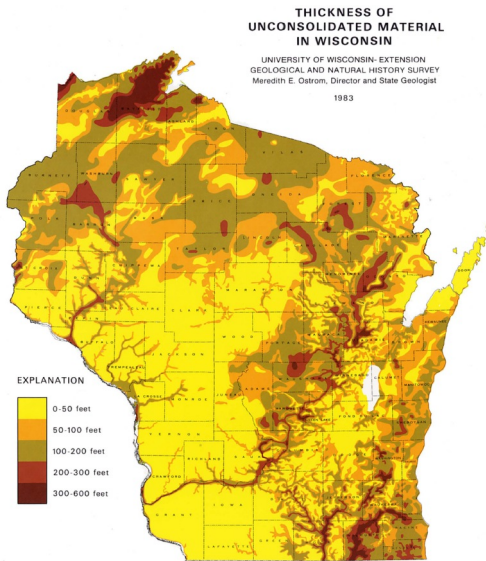


Figure 49 - Thickness of Unconsolidated Material in the State of Wisconsin (Wisconsin Geological and Natural History Survey 2011)

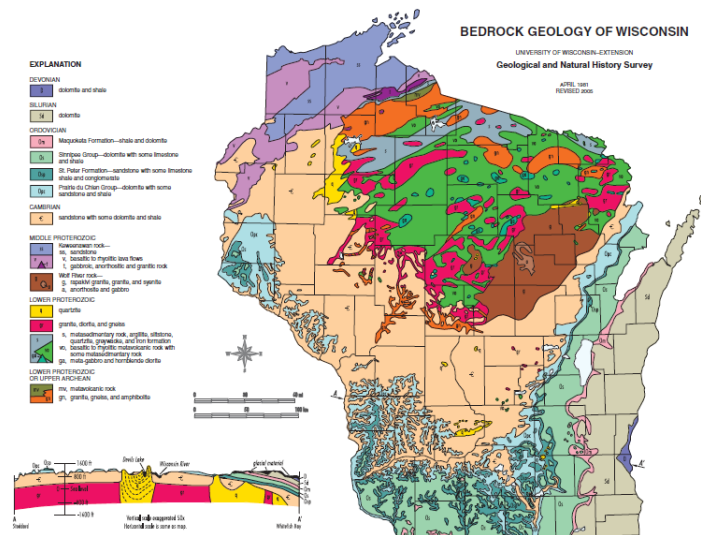


Figure 50 - Bedrock Geology for the State of Wisconsin (Wisconsin Geological and Natural History Survey 2011)

Shaft resistance values are dependent upon soil texture, overburden pressure and soil cohesion. For the State of Wisconsin with the sandy, silty and loamy surface layers of the soil, the average value for the nominal shaft resistance can be approximately chosen as 800 psf (WisDOT 2011). However, experience in Wisconsin

has shown that shaft resistance values reach their constant final values roughly at the depth 20 to 30 times the pile diameter in limited portions of the state, where there is fairly uniform sands of medium density. As an illustration, for a pile with 10-3/4 in. diameter and 40 ft. length, the nominal shaft capacity is approximately equal to 70 kips. On the other hand, the maximum point resistance, or the end bearing capacity of a pile can be estimated based on the simple formulation derived from AASHTO LRFD (AASHTO 2010) (Equation 15).

$$R_p = q_L \cdot A_p \quad \text{Equation 15}$$

where A_p is the pile end area in ft^2 and q_L is the limiting unit point resistance from LRFD [Fig. 10.7.3.8.6f-9] in ksf. According to the dominant composition of the Wisconsin's bedrock (dolomite, granite, and sand stone), the average value for the limiting unit point resistance can be chosen as 300 ksf, considering the average value of 35 to 40 for the corresponding angle of friction. Therefore, for a 10-3/4 in. diameter pile the nominal end capacity is approximately equal to 190 kips. Consequently, the total nominal capacity of the pile, derived from the shaft resistance as well as the end bearing is equal to 260 kips. This value is close enough to the non-composite nominal capacity of the corresponding piles, (see Table 9) providing the opportunity to justify the elastic behavior of the piles prior to the governing mode of the failure related to the soil bearing.

As long as the soil bearing capacity dominated the global behavior of the soil-pile system, the piles behave elastically in the corresponding region. Therefore, the interaction between soil and the pile can be investigated considering only the surrounding soil. In this regards, a spring model was utilized to simulate the effect of surrounding soil on the behavior of the pile structure. As illustrated in Figure 51, the pile is assumed to be embedded in the continuum environment of the soil, with a cylindrical configuration.

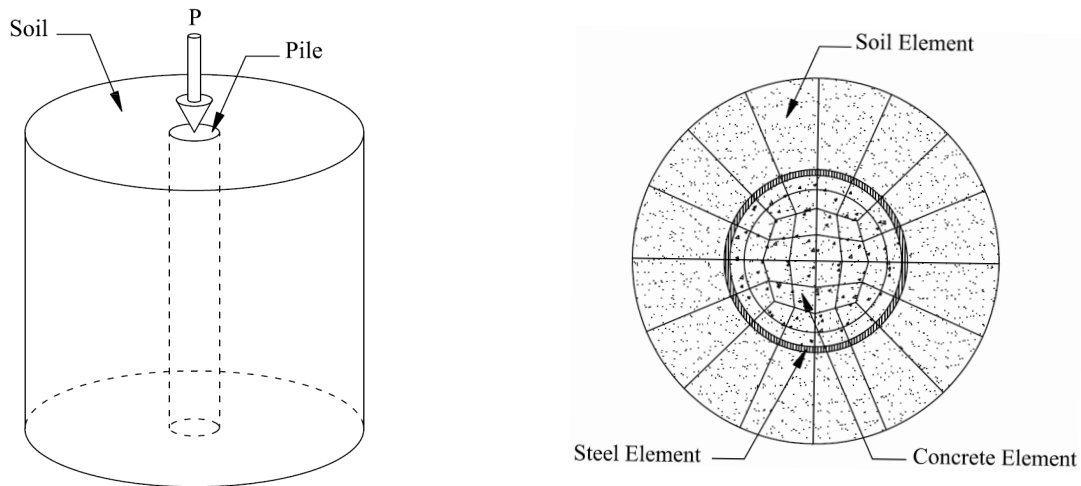


Figure 51 - 3D representation of the pile-soil simulation

Under the applied axial loading of the pile, the soil itself undergoes three sources of deformations (see Figure 52), which can be categorized as follows:

- 1) Vertical Compaction (Δ_{VC}).
- 2) Vertical Shear Deformation (Δ_{VS}).
- 3) Horizontal Compaction (Δ_H).

Each of these deformation components is related to the stiffness of the soil in the corresponding directions. Moreover, these stiffnesses can be represented by means of linear longitudinal springs for the numerical simulation purposes.

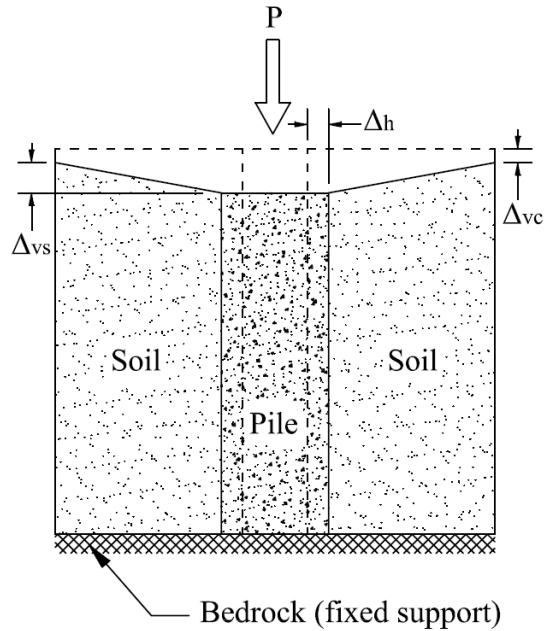


Figure 52 - Soil – pile deformation under applied load

Consequently, the following model, presented in Figure 53, was developed to derive each of the stiffness components of the soil with respect to the geometry of the simulated cylinder of the surrounding soil. It should be mentioned that the accuracy of the results is not affected by the mesh size, but it can be influenced by the dimension (radius) of the soil cylinder (see Figure 51).

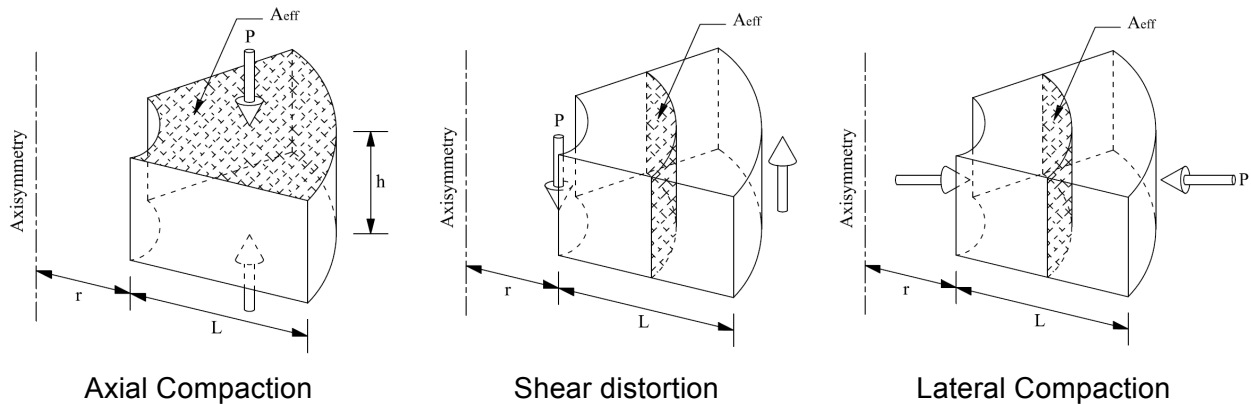


Figure 53 - Proposed numerical model to derive the equivalent spring stiffness of the soil

The equivalent spring stiffnesses for all components of deflections are calculated as given in Equation 16.

$$\begin{aligned}
K_{VC} &= \frac{E}{h} \times \frac{1}{2} \theta \times r^2 \times (n^2 + 2n) & \text{(a) Vertical Compaction} \\
K_{VS} &= \frac{G}{L} \times \frac{1}{2} \theta \times r \times h \times (n+2) & \text{(b) Shear Disturion} \\
K_H &= \frac{E}{L} \times \frac{1}{2} \theta \times r \times h \times (n+2) & \text{(c) Lateral Compaction}
\end{aligned}
\tag{Equation 16}$$

where E is the elastic modulus of the surrounding soil, G is the shear modulus of the surrounding soil, θ is the central angle, h is the height of the of the soil element with respect to the mesh generation, r is the radius of the pile, L is the radial length of the surrounding soil, and n is the ratio between L and r . It should be mentioned that K_{VC} and K_{VS} are in series with each other and can be combined to have an equivalent vertical spring with an equivalent stiffness, K_V , derived as given by Equation 17:

$$K_V = \frac{K_{VC} \times K_{VS}}{K_{VC} + K_{VS}}
\tag{Equation 17}$$

For the numerical simulation purposes, the surrounding soil, previously idealized as a series of horizontal and vertical linear longitudinal springs, are introduced to the 3D FE model as depicted in Figure 54.

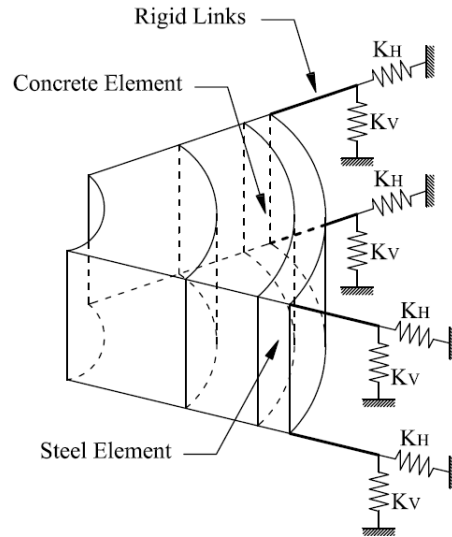


Figure 54 - FE representation of soil - pile interaction

In order to reduce the computational cost, only a quarter of the pile's stub sections were simulated and the appropriate boundary conditions as well as the equivalent lateral springs were also applied to satisfy the symmetry conditions, as depicted in Figure 55.

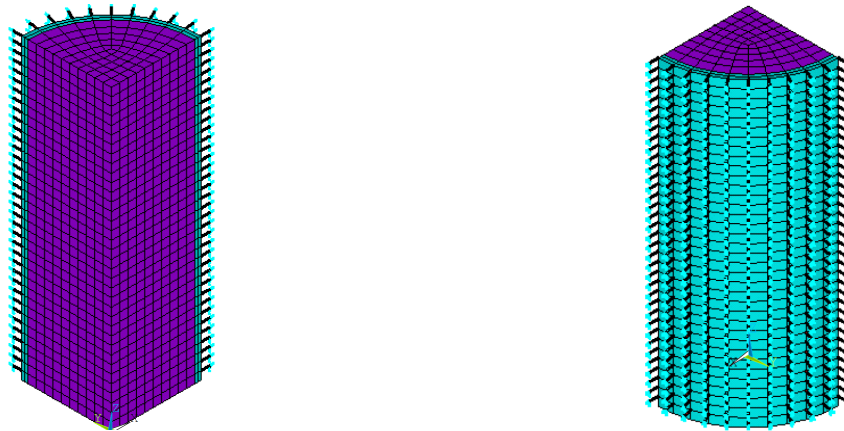


Figure 55 - FE simulation equivalent soil springs

Considering the dominant type of soil in the State of Wisconsin, loose and compact sandy as well as gravel soil were chosen for the numerical analysis. The corresponding values of the equivalent lateral stiffness are presented in Table 11 for a certain type of mesh generation.

Table 11 - Equivalent lateral stiffness of the surrounding soil

Soil type	E (ksi)	G (ksi)	K_H (k/in)	K_V (k/in)
Loose sandy soil (LSS)	1.45	0.58	0.08	0.03
Compact sandy soil (CSS)	7.25	2.59	0.40	0.14
Loose Gravel soil (LGS)	10.15	4.41	0.56	0.24
Compact Gravel Soil (CGS)	24.66	9.13	1.36	0.50

For all of the previous specimens, the load was applied concentrically to a maximum level of 1000 kips, the capacity of the testing frame. For the first series of the analysis, the soil type and the thickness of the surrounding soil were considered to be fixed, in order to investigate the effect of concrete compressive strength on the soil - pile interaction. Accordingly, the loose gravel soil with the thickness of 5 times the radius of the embedded pile was chosen for the analysis. The corresponding longitudinal and tangential strain distributions are depicted in Figure 56, derived from ANSYS as an output contour. Figure 57 - Figure 59 also illustrates the load vs. longitudinal strains as well as tangential strains for all specimens with different geometrical properties. By converting applied loads into longitudinal stress using section transformation, the effective applied stress vs. longitudinal and tangential strains is also depicted in Figure 60 - Figure 62 for a comparison of stress-strain response among different piles. As it can be seen, the surrounding soil does not have a significant effect on the behavior of the pile within the elastic limit, for different types of concrete.

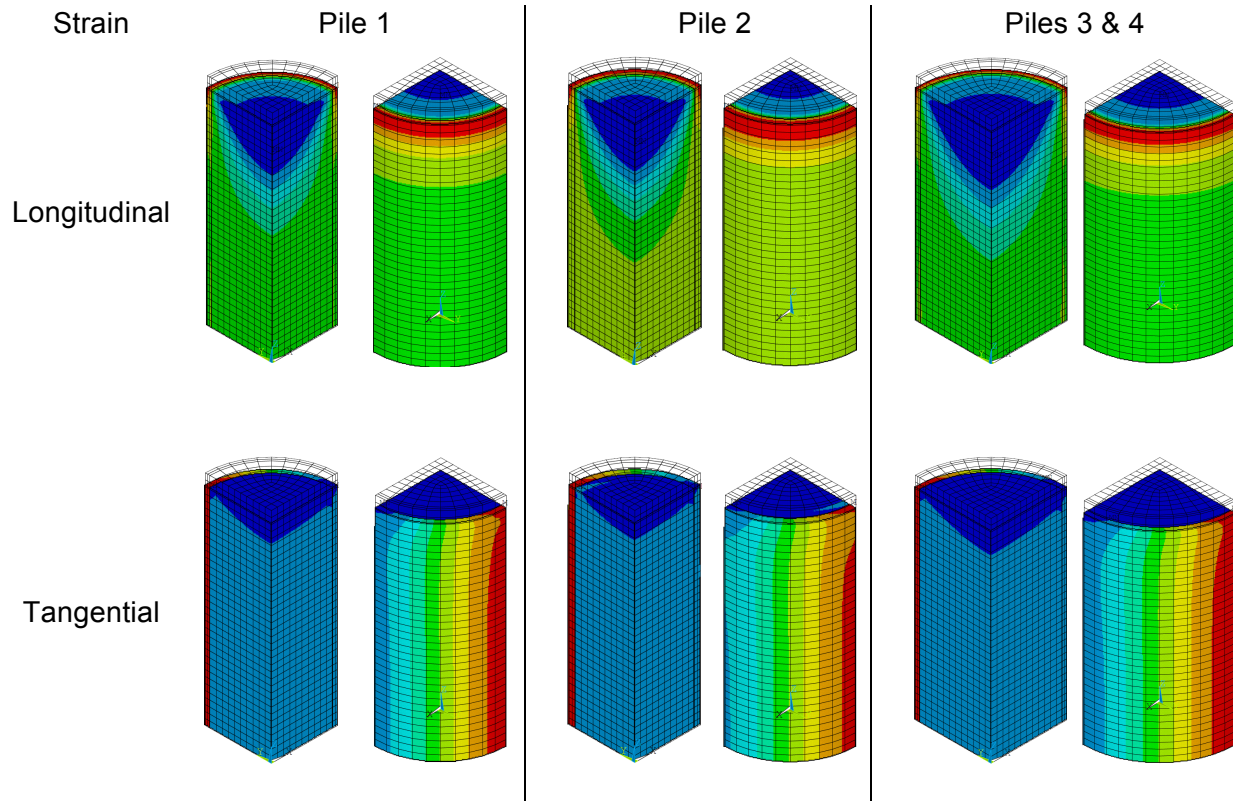
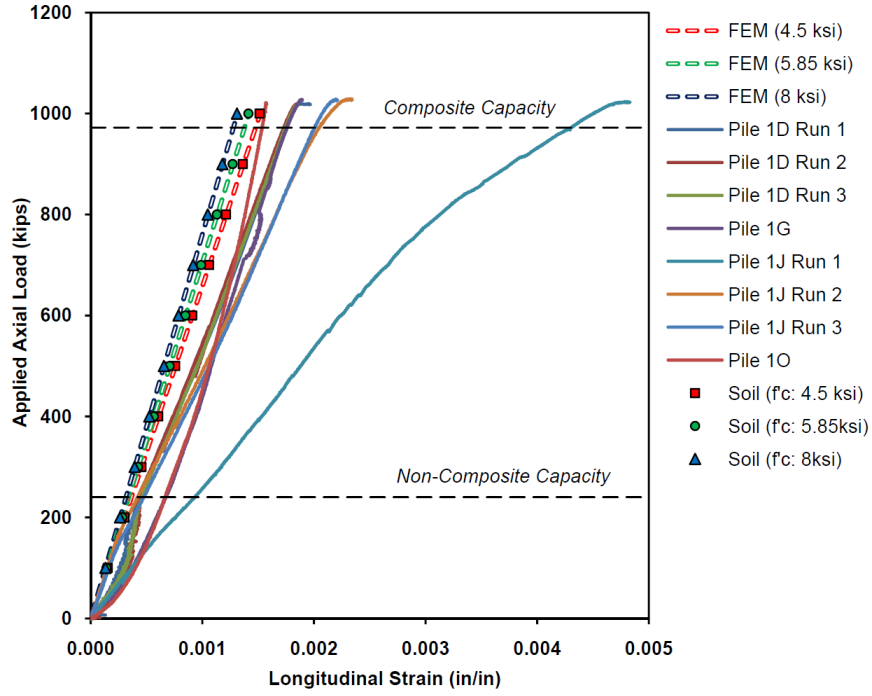
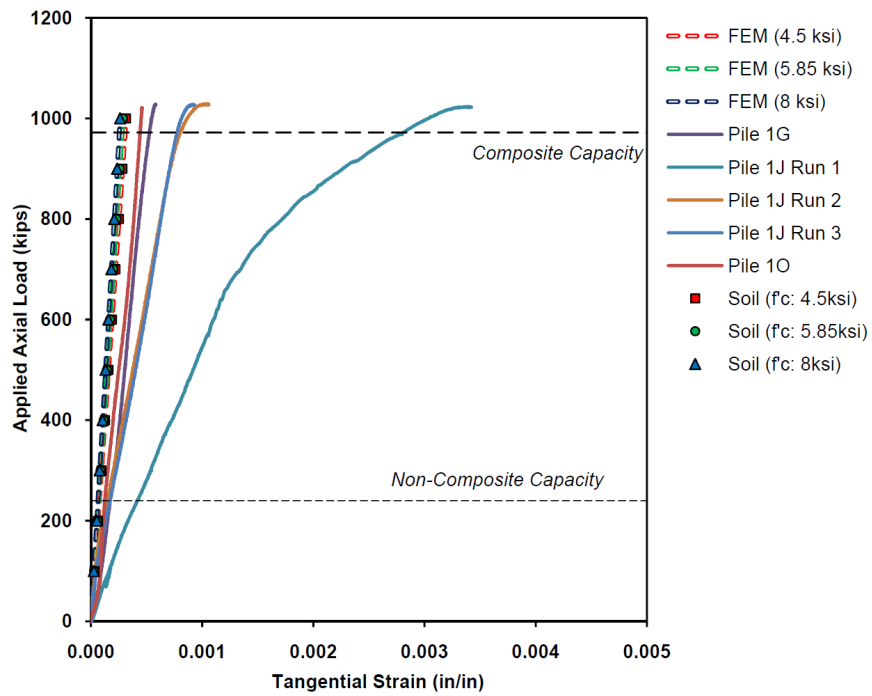


Figure 56 - Strain distribution contours considering soil - pile interaction

For the second part of the analysis, the effect of soil material properties on the behavior of the cast-in-place tubular pile was investigated. It should be mentioned that the other sensitive parameters such as soil thickness (defined by n), compressive strength of the concrete, and diameter of the pile were considered to be fixed for this study. The results obtained from the numerical analysis indicated that the surrounding soil does not have a significant effect on the behavior of the pile as long as the pile responses are located within the elastic limit, even for different types of the soil properties.

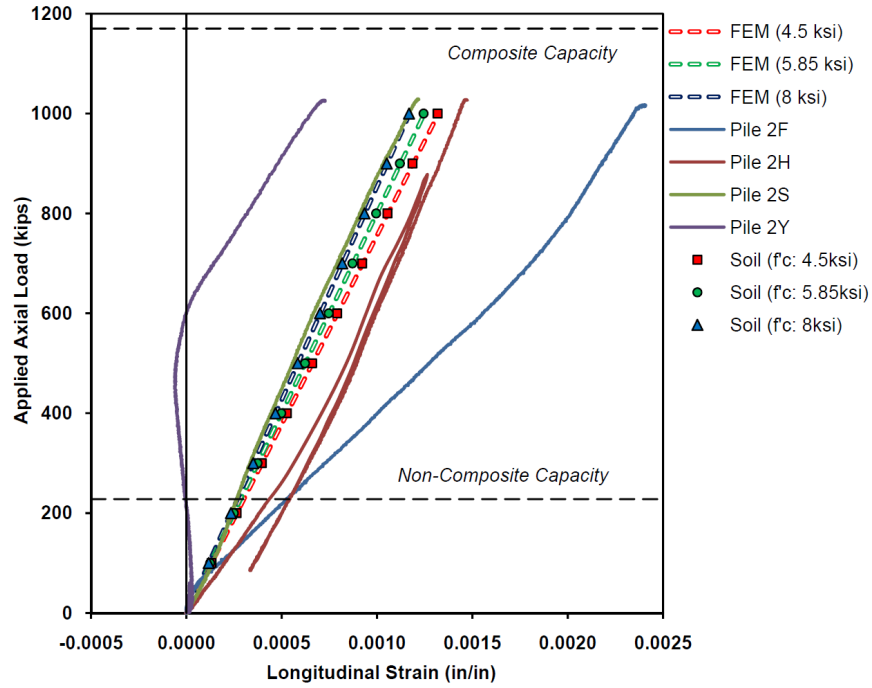


a)

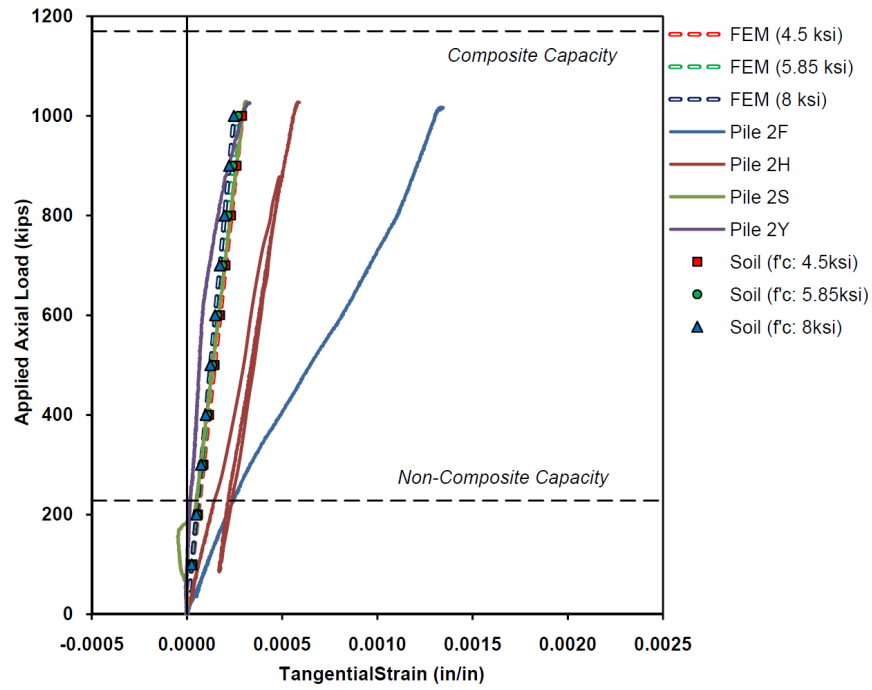


b)

Figure 57 - Pile 1 (10.75" - 0.375" wall) Load (composite) vs. a) longitudinal strain, b) tangential strain – with soil-pile interaction

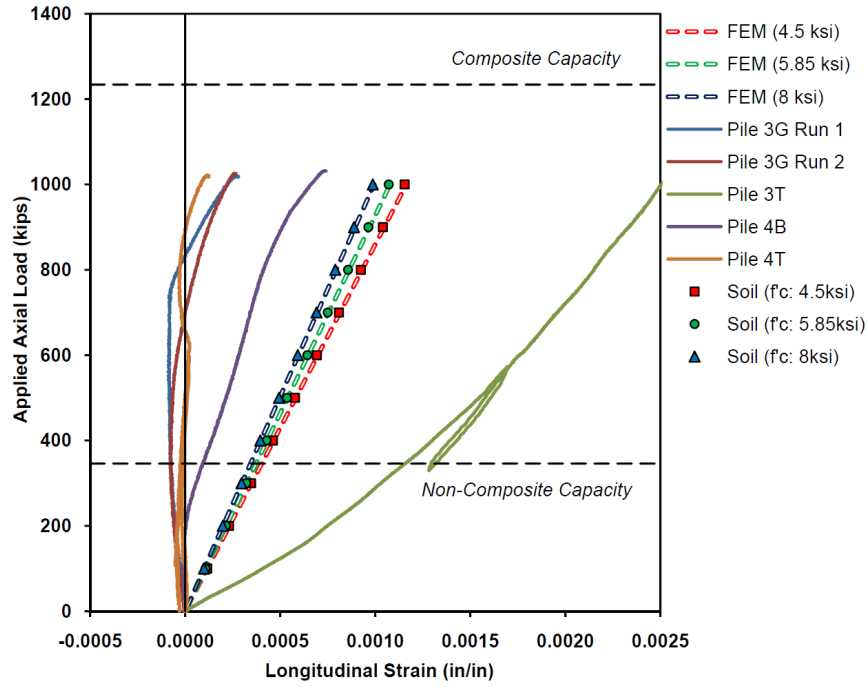


a)

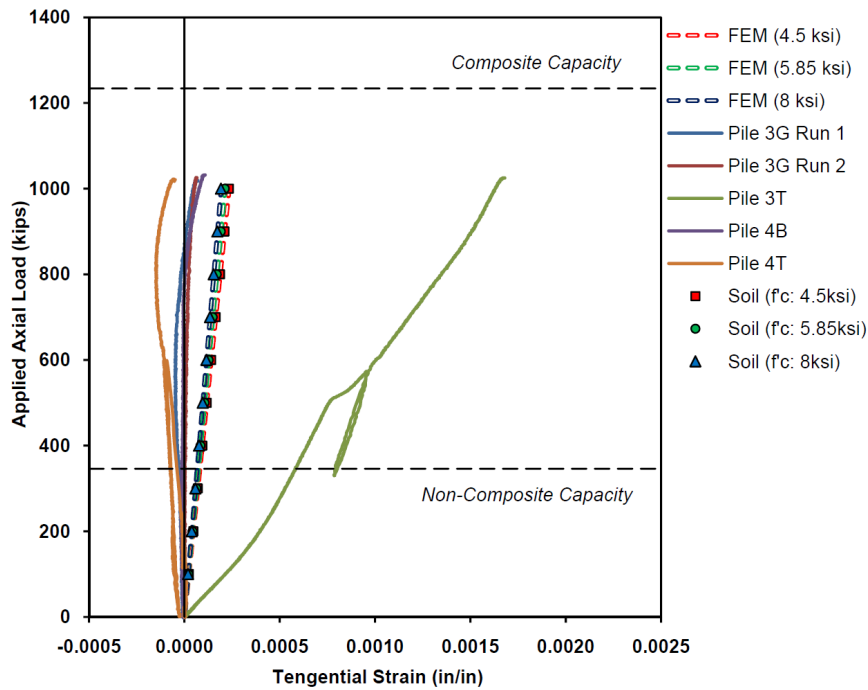


b)

Figure 58 - Pile 2 (10.75" - 0.5" wall) Load (composite) vs. a) longitudinal strain, b) tangential strain – with soil-pile interaction

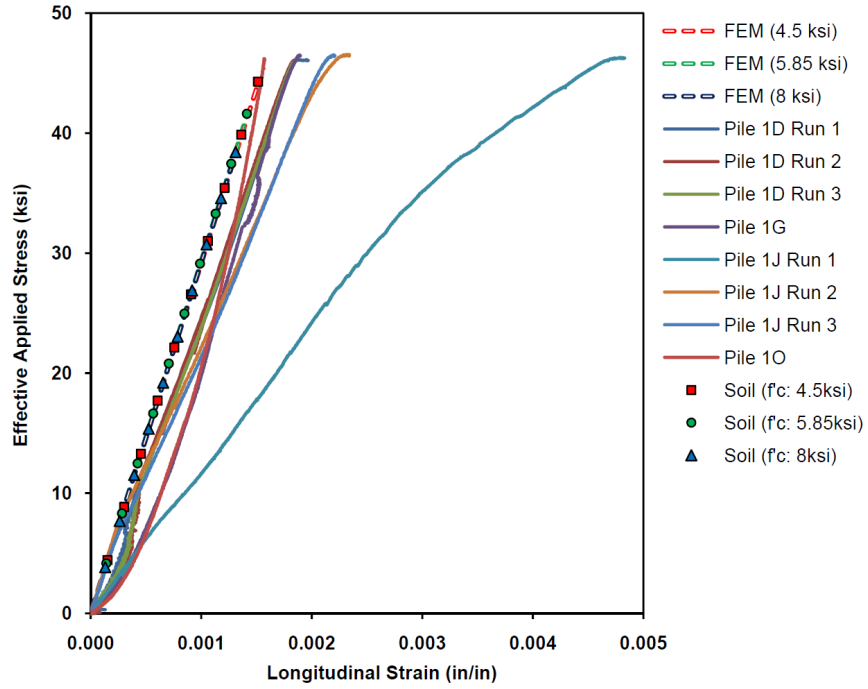


a)

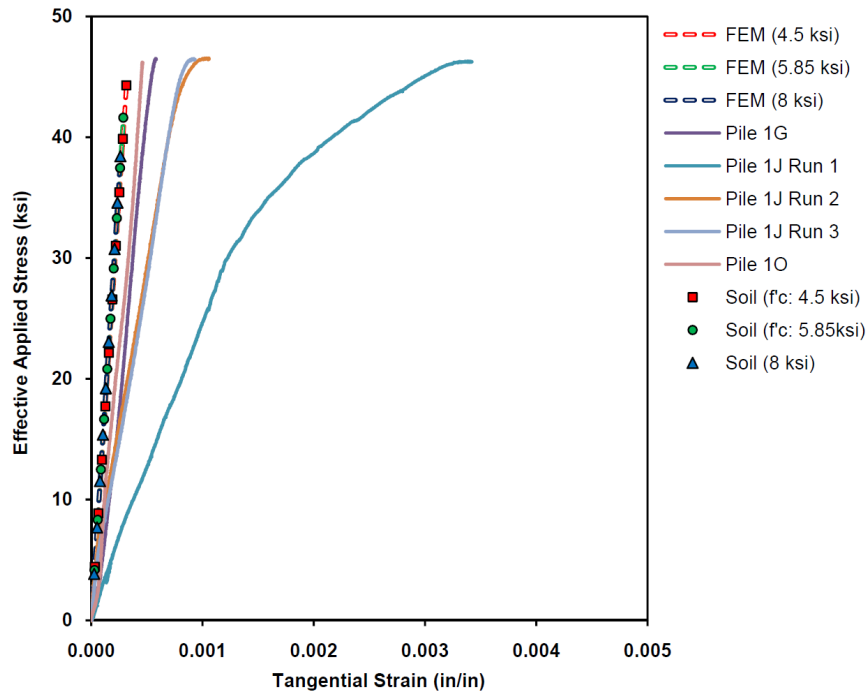


b)

Figure 59 - Piles 3 & 4 (12.75" - 0.375" wall) Load (composite) vs. a) longitudinal strain, b) tangential strain – with soil-pile interaction

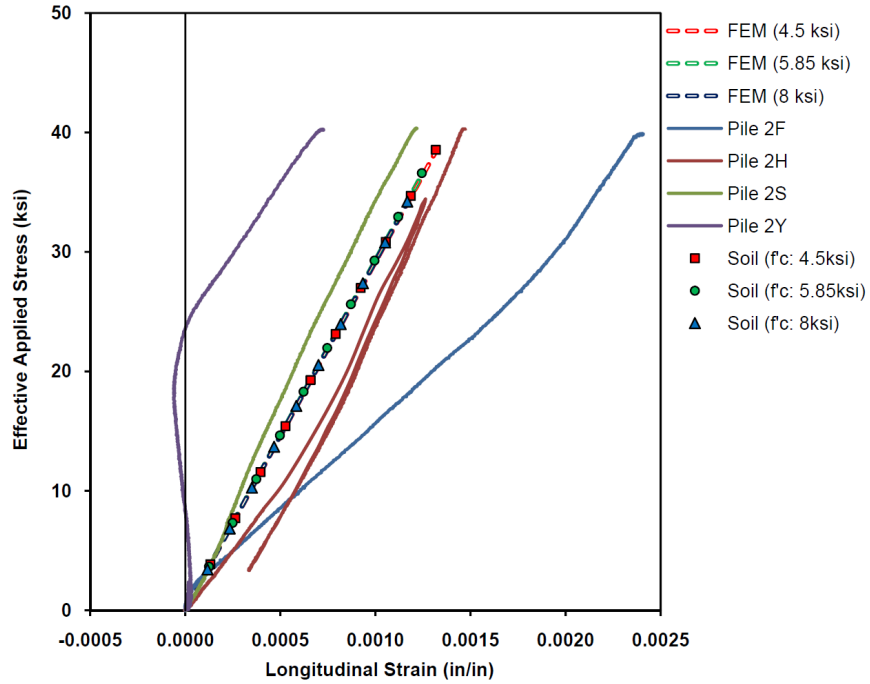


a)

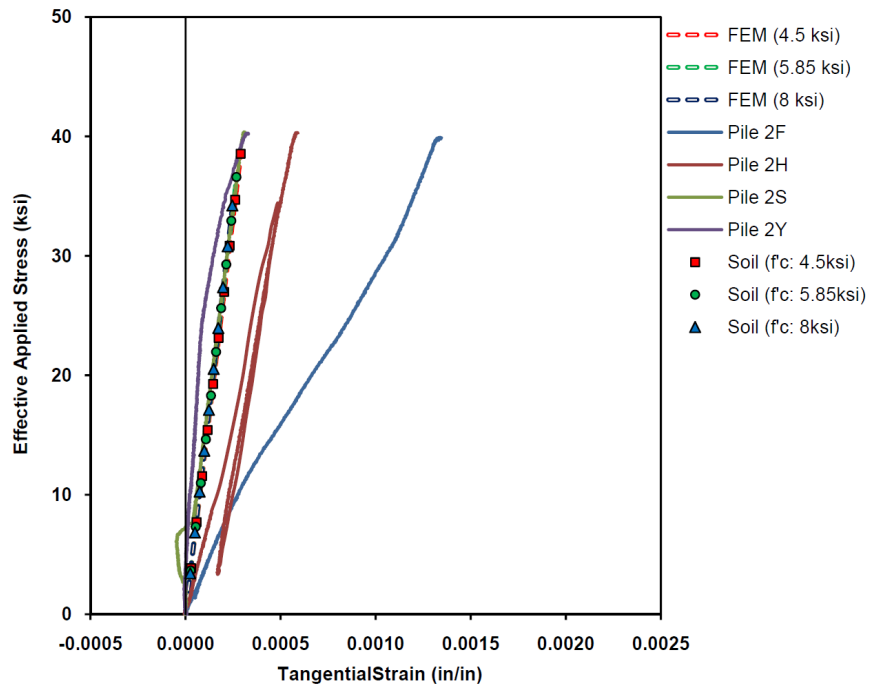


b)

Figure 60 - Pile 1 (10.75" - 0.375" wall) Effective stress (composite) vs. a) longitudinal strain, b) tangential strain – with soil-pile interaction

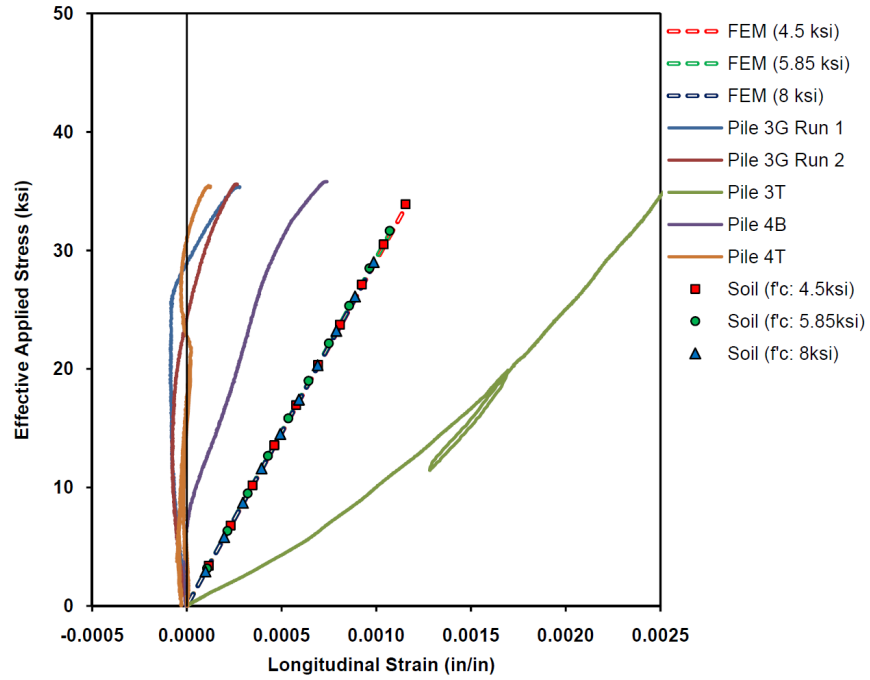


a)

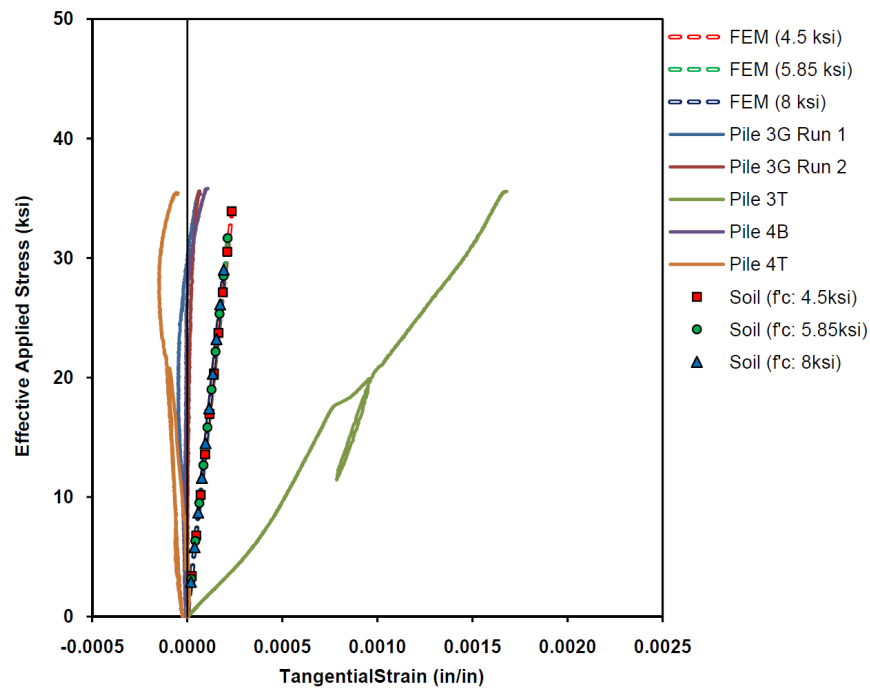


b)

Figure 61 - Pile 2 (10.75" - 0.5" wall) Effective stress (composite) vs. a) longitudinal strain, b) tangential strain – with soil-pile interaction



a)



b)

Figure 62 - Piles 3 & 4 (12.75" - 0.375" wall) Effective stress (composite) vs. a) longitudinal strain, b) tangential strain – with soil-pile interaction

4.5 Push-Through Testing

This test was designed to determine the strength of the bond between the steel shell and concrete core. If this bond is adequate, composite action would be appropriate for design. This test was intended to determine the load at which the core starts to slide through the steel shell, which is the point at which the bond breaks.

In this test, the load was applied at the same rate as the previous tests, until the load on the section decreased by fifteen percent. The load versus cross head displacement for the 10-3/4" dia. (0.375" wall), 10-3/4" dia. (0.5" wall), and 12-3/4" dia. (0.375" wall) are presented in Figure 63, Figure 64, and Figure 65, respectively. For all of the 10-3/4 in. diameter specimens, the behavior is characterized by an increase in load until the bond is broken, followed by a gradual decrease in load as the concrete core pushes through the shell. Due to the spiral welds in the shell of the 12-3/4 in. diameter samples, the specimens never reach a maximum load or exhibited a load drop off. Instead the core started to move and came in contact with another weld seam, which was not flush on the interior. This caused the load to increase again causing a small displacement until the core hit the spiral weld seam again. For all specimens, the bond strength was calculated as the peak load at the initial slip divided by the internal surface area. The average bond strengths for each specimen cross sections are presented in Table 12. These values for the bond strengths are on the low end of the bond strengths when compared with previous research, which show that the bond strength can vary from 0.3 ksi to around 2 ksi (Harajli 2004) for concrete and deformed bars and between 0.34 to 0.48 ksi for smooth bars (Menzel 1939; Weathersby 2003). However, it should be noted that these bond strengths are based on bond of concrete to deformed bars (reinforcing steel) and the pile sections have smooth steel walls.

Some notable findings from these tests were that the bond varied between the sections, the largest section did not have the strongest bond, and the bond varied with depth of the pile. The fact that the largest section did not have the strongest bond could have been due to the weld seam impeding on the contact surface of the materials. Each sample tested was taken from various locations through the depth so that the average bond for the type of shell could be found. The capacity of the bond is on the

lower end for concrete to steel, however none of the compression tests exhibited any type of shell/core separation or observable slip during loading. While no measurement of the shear stress at the interface was measured during the compression testing, the shear stresses at the interface from the finite element models ranged from 0.011 – 0.024 ksi for the composite section loading. For the core only loading scenario, the shear stress ranged 0.825 – 5.617 ksi, however this loading scenario is unlikely to be observed in service due to the pile cap being cast over the entire pile rather than just the core section. These stresses suggest that the interface bond capacity is sufficient for the expected state of stress for in-service conditions.

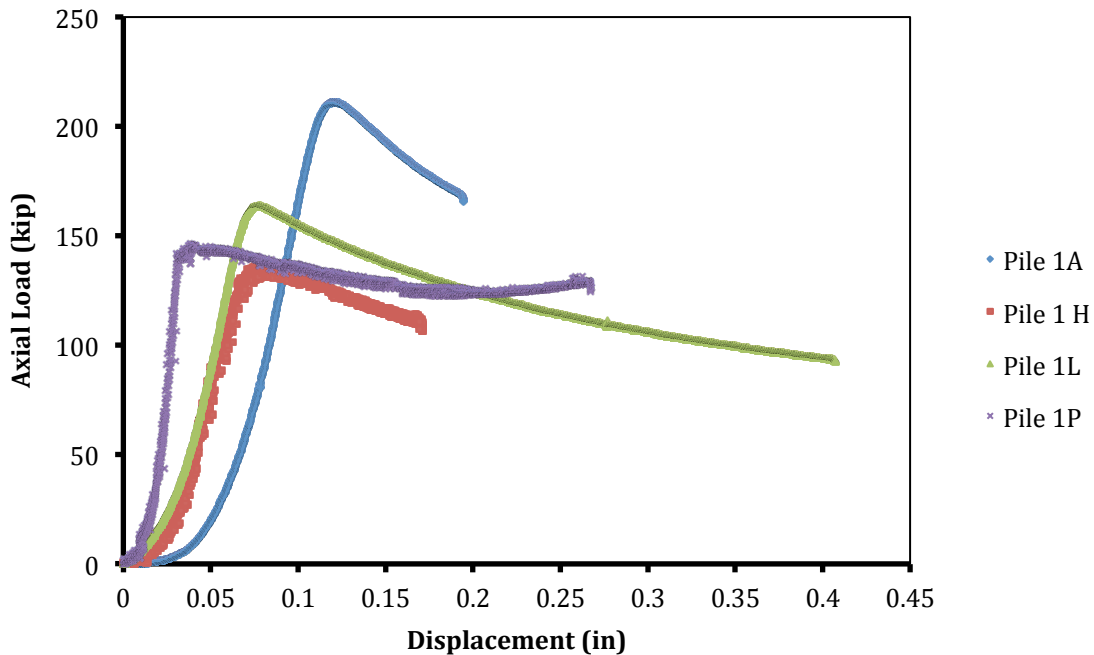


Figure 63 - Bond Strength – 10-³/₄" (0.375" wall)

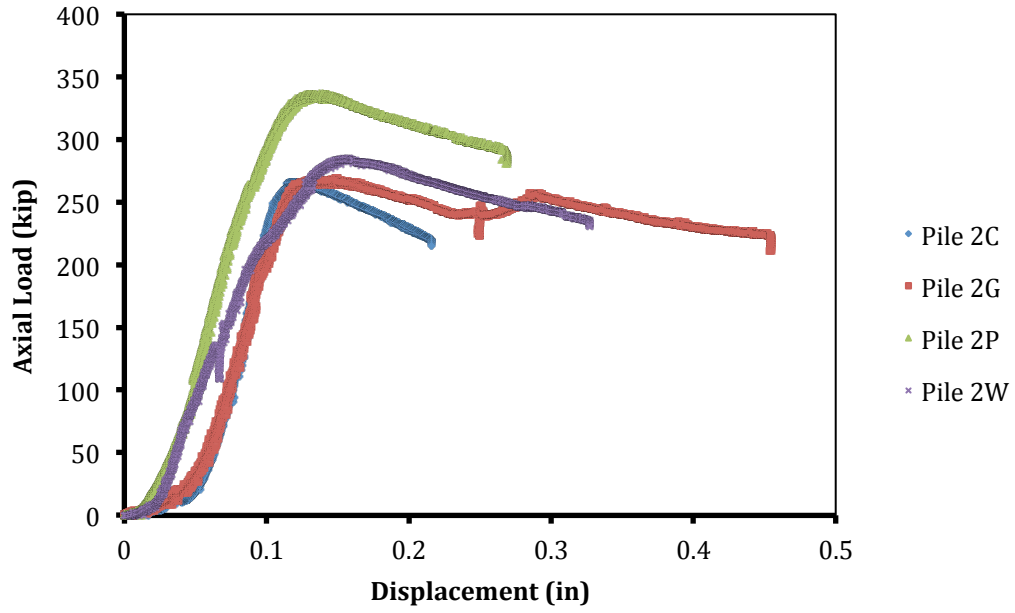


Figure 64 - Bond Strength – 10-³/₄" (0.5" wall)

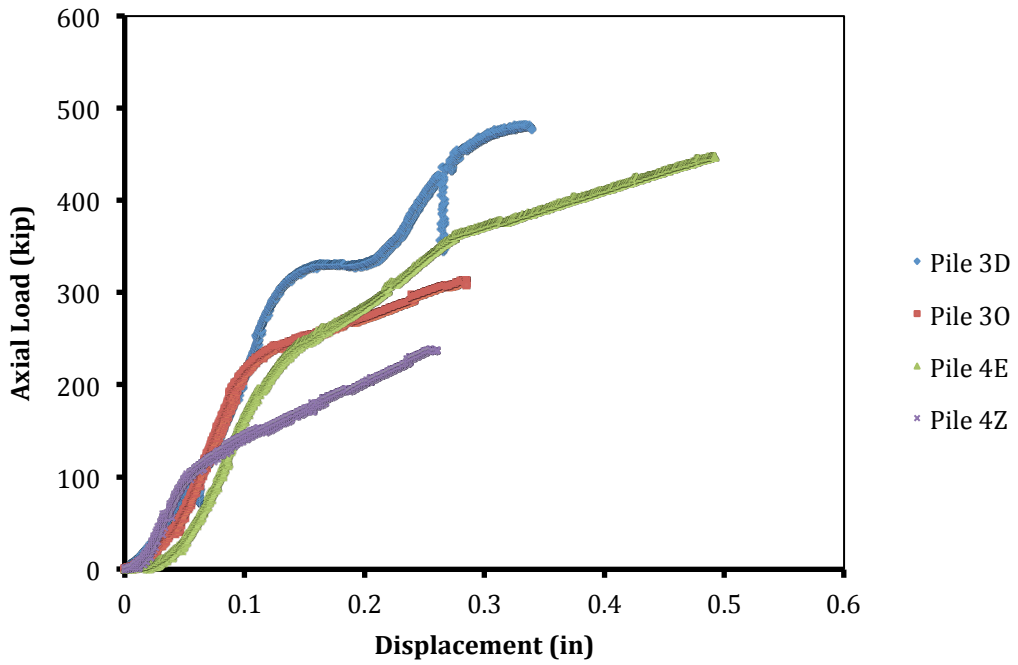


Figure 65 - Bond Strength – 12-³/₄" (0.375" wall)

Table 12 - Concrete-Steel Bond Strength

Specimen Name	Depth (ft.)	Pile Size	Bond Strength (ksi)	Average (ksi)
1A	1.5	10-3/4" dia. (0.375" wall)	0.373	0.291
1H	11.5		0.241	
1L	17.5		0.289	
1P	23		0.259	
2C	4.5	10-3/4" dia. (0.5" wall)	0.483	0.525
2G	10		0.489	
2P	25.5		0.611	
2W	36		0.517	
3D	5.5	12-3/4" dia. (0.375" wall)	0.451	0.316
3O	21.5		0.317	
4E	8.5		0.339	
4Z	40		0.157	

4.6 Flexural Testing

Flexural testing (three point loading configuration) was performed on the four 11 ft. long pile sections. In this test, the load was applied at a constant rate with the objective of the evaluation focused on the performance of the concrete core – steel shell interface. The strain gauges mounted on the perimeter were intended to assess the degree of composite action between the two materials and to determine if there was a loss of bond in a flexural scenario. Results from the experimental program are presented in two forms, a strain versus loading and a change in strain through the cross-section depth. It was expected that the former would indicate a change in section behavior (e.g. cracking, loss of bond) while the latter would highlight the location of this change. Results from the LVDT measurements of end-split are not included in this report because none were measured during the testing.

12-3/4" dia. (0.375" wall) – Pile 3

The combined strain vs. load plot for the first 12-3/4 in. diameter pile is presented in Figure 66 (tension strain positive). As expected the general trend is a proportional increase in strain with load for all measurements with the exception of those located at

the neutral axis. From Figure 67, a noticeable shift in linearity occurs between 25-35 kips, indicating a change in system behavior (as noted by the box on the figures). Figure 68, highlights this region further and suggests that this change occurs at ~26 kips. When comparing the strain through the depth of the cross-section for this loading region, it becomes evident that cracking on the tension side in the lower right quarter results because of the shift in strain distribution. However, no slip was observed at the locations of the interface gauges near the neutral axis where maximum shear is expected.

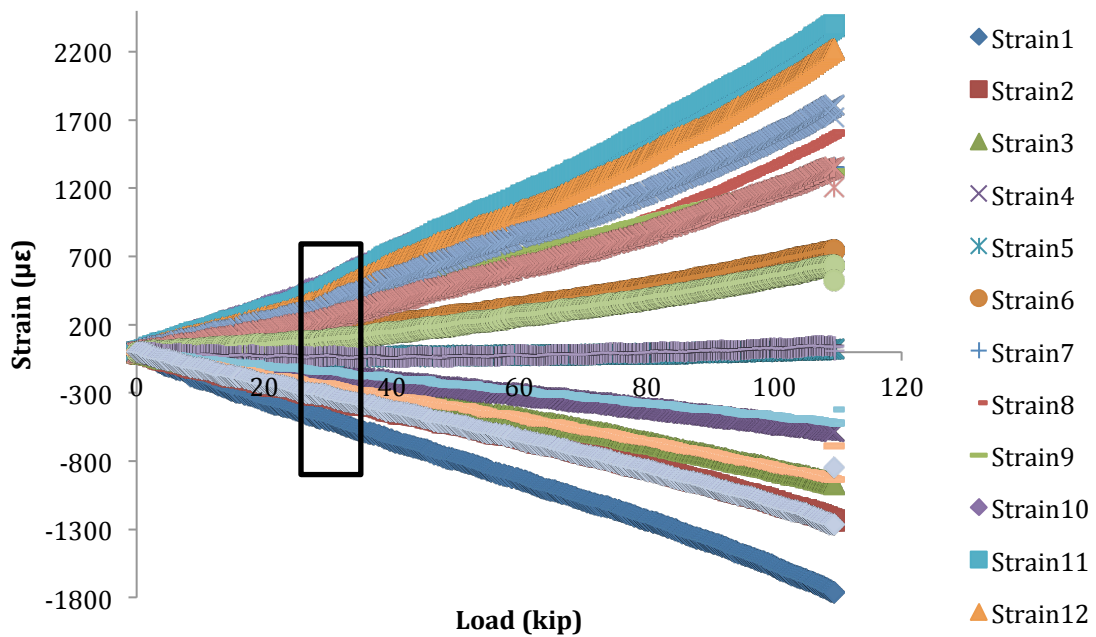


Figure 66 – Strain vs. load (all gauges) for (12-3/4" – 0.375" wall) – Pile 3 (full range of loading)

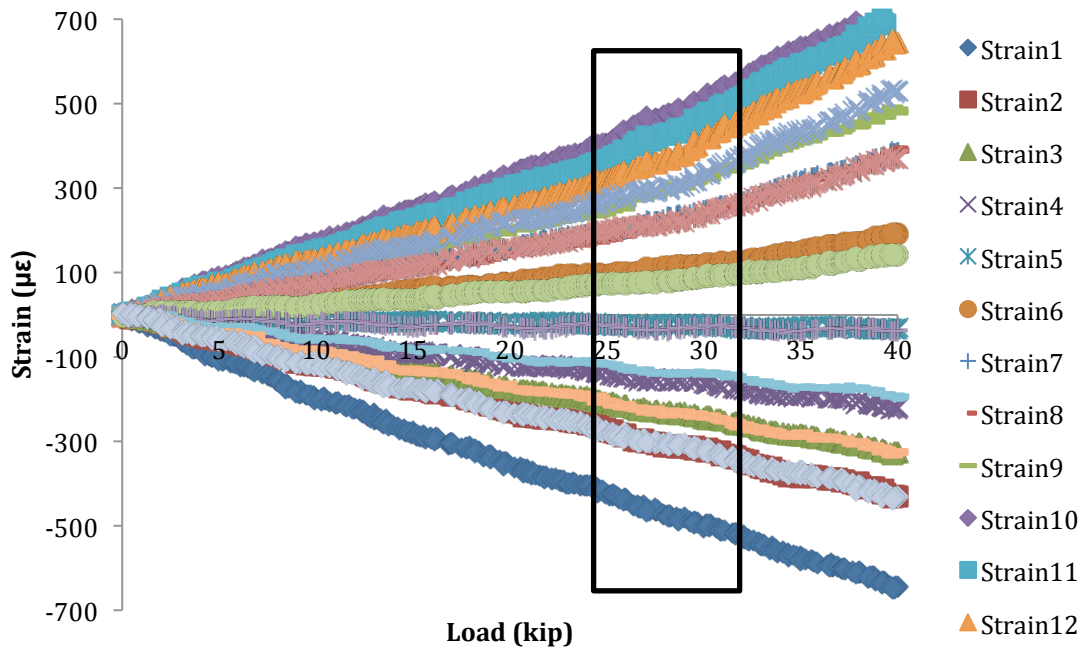


Figure 67 - Strain vs. load (all gauges) for (12-3/4" – 0.375" wall) – Pile 3 (partial range of loading)

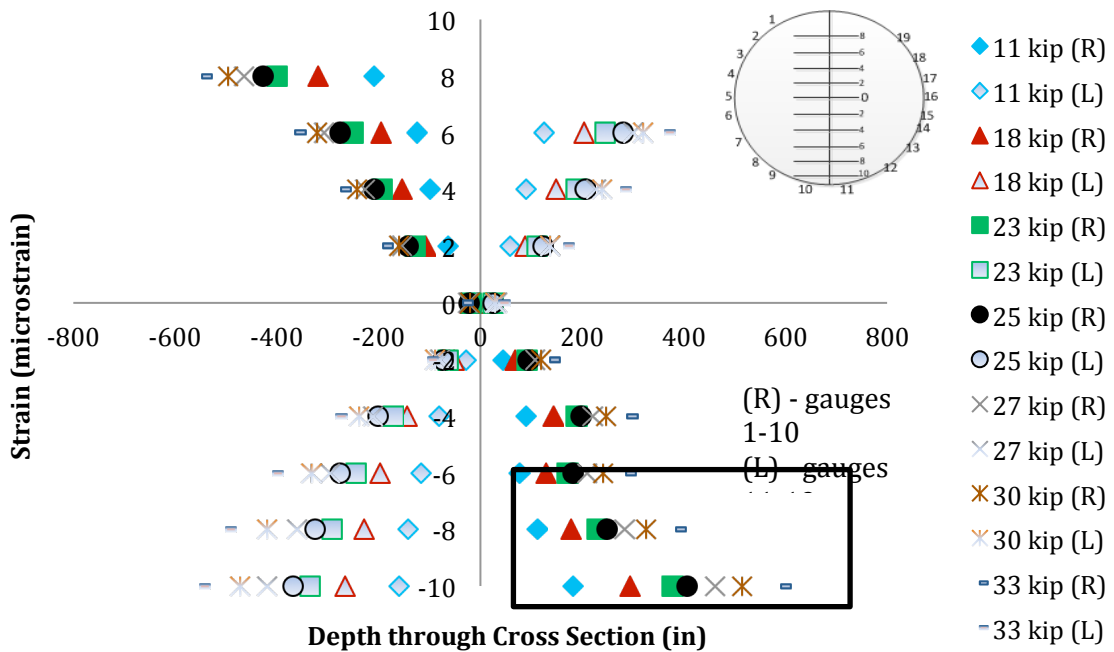


Figure 68 - Strain vs. load through cross-section depth (12-3/4" – 0.375" wall) – Pile 3

12-3/4" dia. (0.375" wall) – Pile 4

The second 12-3/4 in. diameter pile was tested in a similar manner as the first and was loaded to the capacity of the test frame. Similar to Pile 4 a general observed trend is a proportional increase in strain with load for all measurements with the exception of those located at the neutral axis. For this specimen, the load was applied to the center, which coincided with a weld seam. From Figure 69, a noticeable shift in linearity occurs between 20-40 kips, indicating a change in system behavior. Figure 70, highlights this region further and suggests that this change occurs at ~24 kips. When comparing the strain through the depth of the cross-section for this loading region (Figure 71), the change in slopes on the tension side is less evident than Pile 3, which can likely be attributed to the load being applied to the weld seam, resulting in a non-uniform distribution of stress. For this specimen, no slip was observed at the locations of the interface gauges where maximum shear is expected, near the neutral axis.

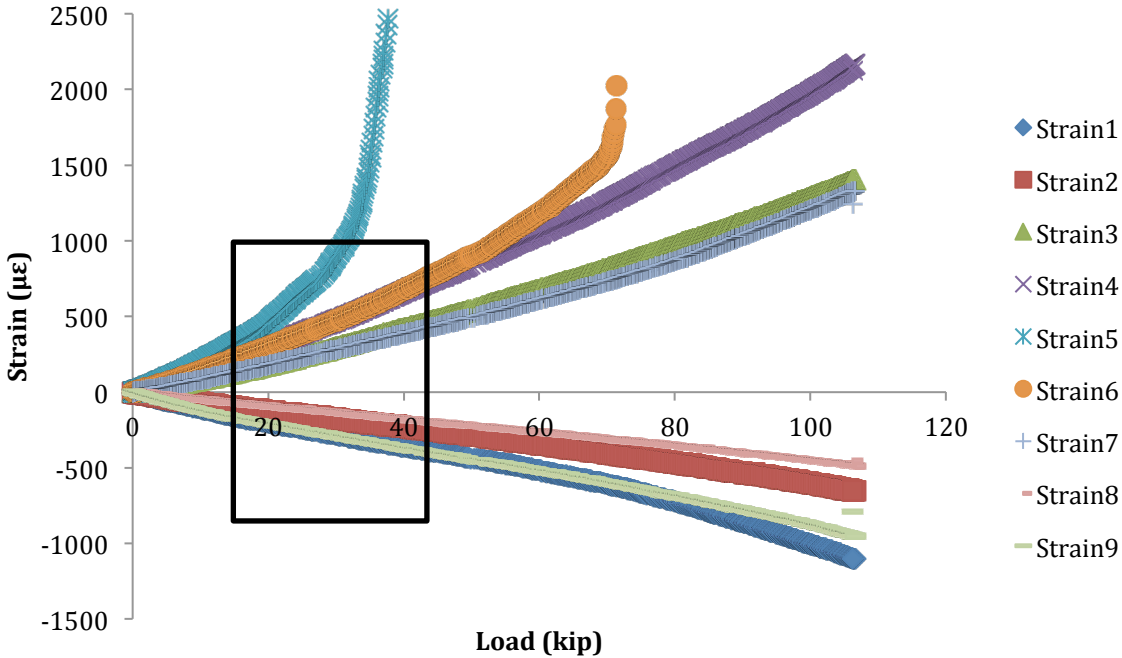


Figure 69 - Strain vs. load (all gauges) for (12-3/4" – 0.375" wall) – Pile 4 (full range of loading)

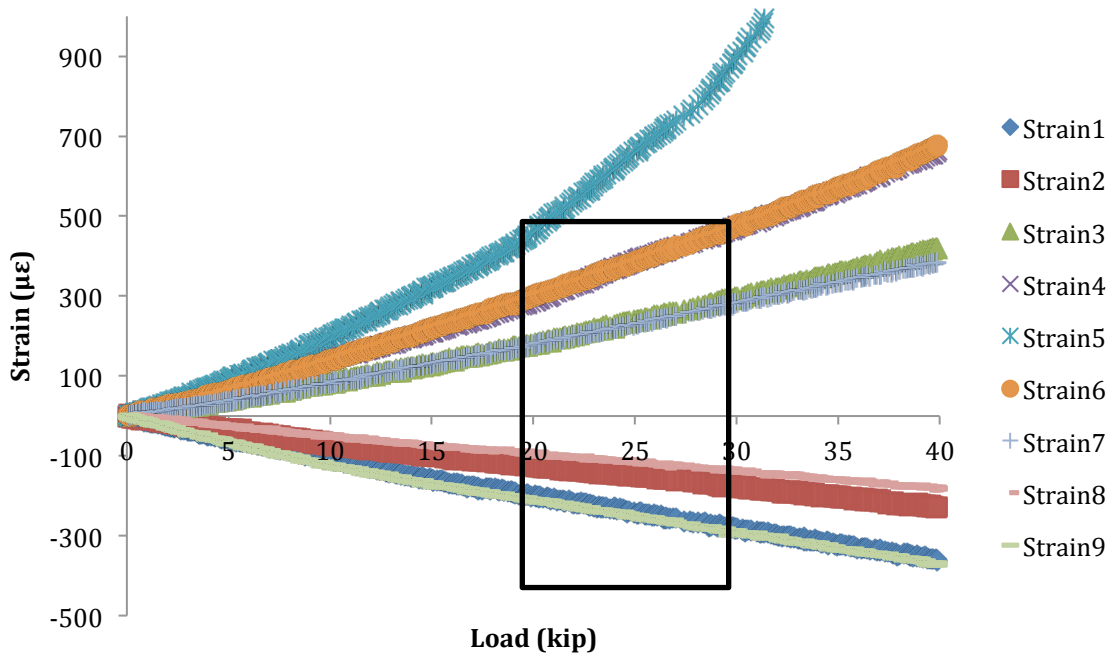


Figure 70 - Strain vs. load (all gauges) for (12-3/4" – 0.375" wall) – Pile 4 (partial range of loading)

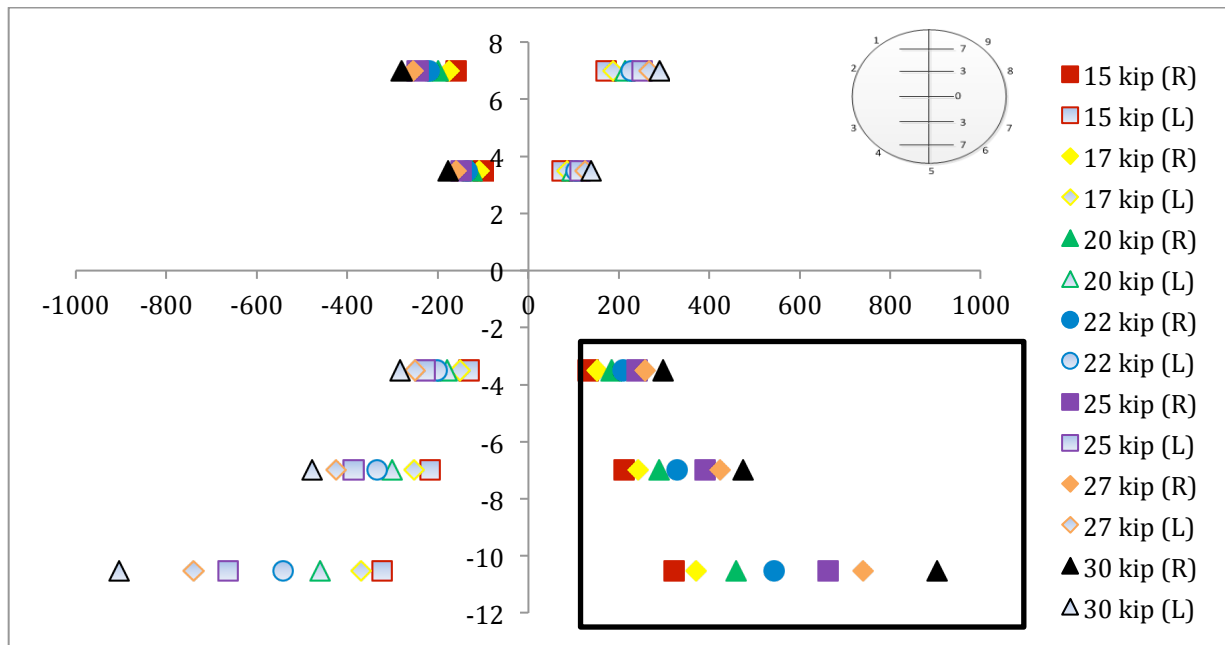


Figure 71 - Strain vs. load through cross-section depth (12-3/4" – 0.375" wall) – Pile 4

10-3/4" dia. (0.375" wall) – Pile 1

Pile 1 (10-3/4" dia. – 0.375" wall) was tested in flexure to the maximum stroke capacity of the test frame. The complete strain vs. load response is illustrated in Figure 72. For this specimen the deviation in specimen responses was observed at an approximate load of 7 kips (Figure 73). From the load vs. cross-section depth (Figure 74), the cracking again appears to be on the lower side of the specimen, with both sides exhibiting a degree of non-linearity in the strain distribution. This section did fail at the maximum load, ~68 kips, and the failure occurred at one of the weld seams (Figure 75). At failure, the seam between the weld separated and the concrete core also cracked. This location seemed to be the location of maximum stress and made it difficult to detect changes in slope at midspan.

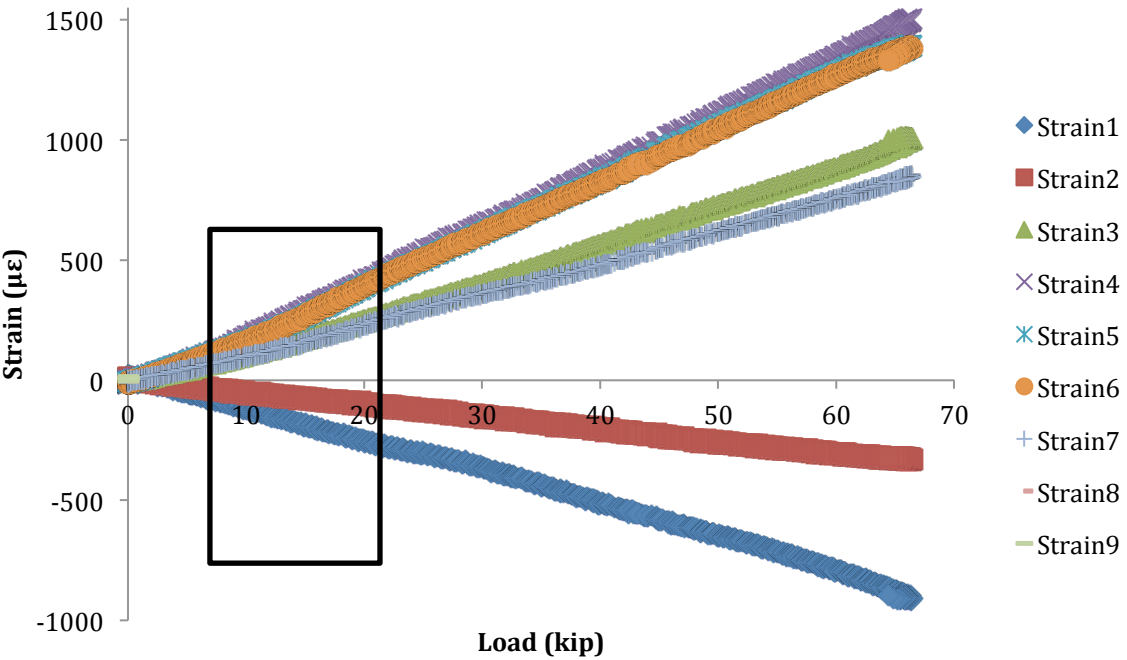


Figure 72 - Strain vs. load (all gauges) for (10-3/4" – 0.375" wall) – Pile 1 (full range of loading)

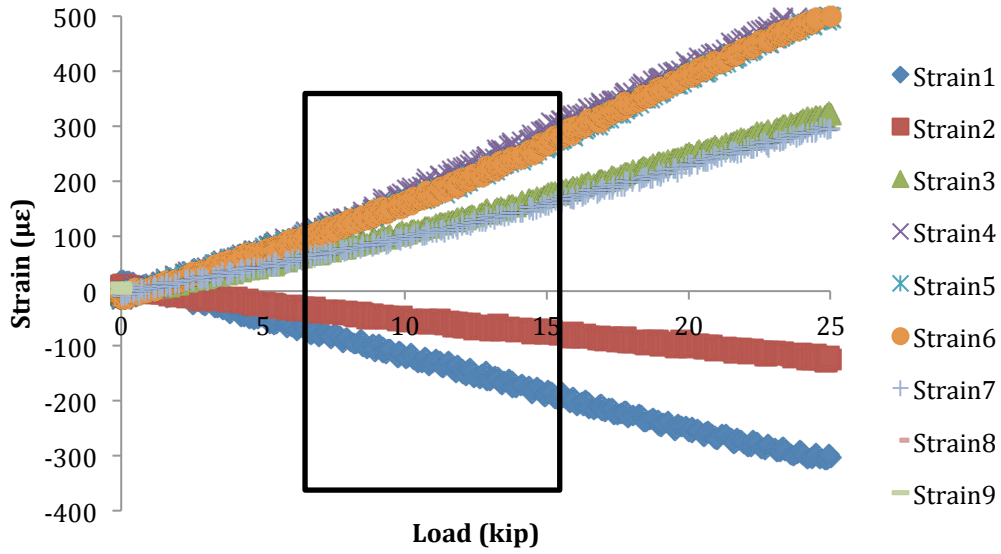


Figure 73 - Strain vs. load (all gauges) for (10-3/4" – 0.375" wall) – Pile 1 (partial range of loading)

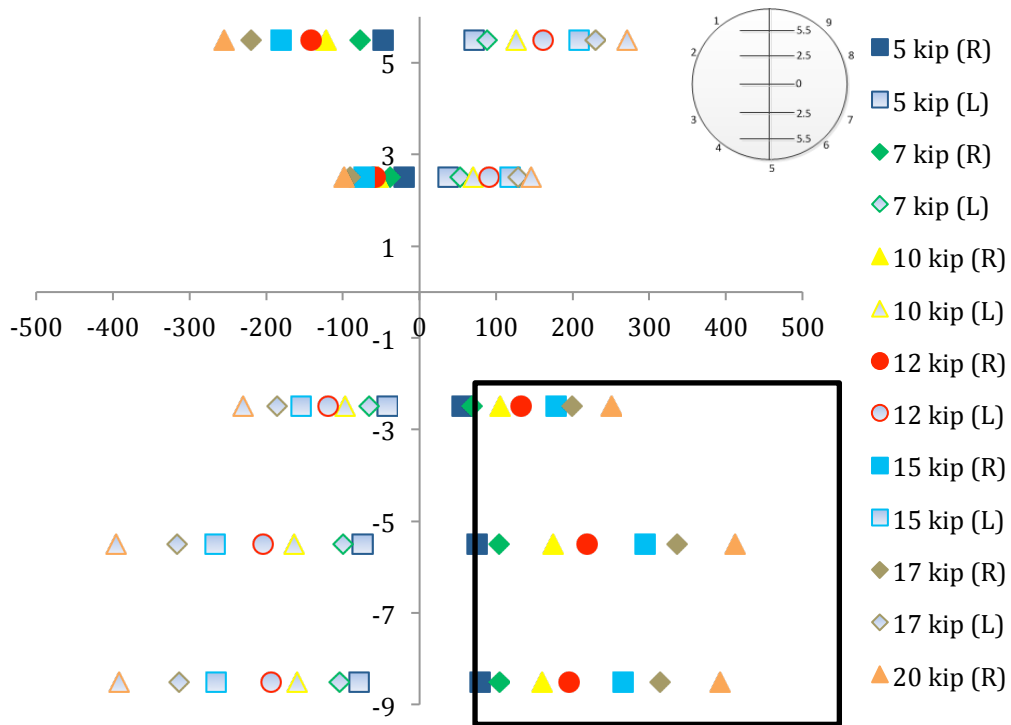


Figure 74 - Strain vs. load through cross-section depth (10-3/4" – 0.375" wall) – Pile 1



Figure 75 – Pile 1 Failure Location

10-3/4" dia. (0.5" wall) – Pile 2

Pile 2 (10-3/4" dia. – 0.5" wall) was tested in flexure to the maximum stroke capacity of the test frame. The complete strain vs. load response is illustrated in Figure 76. For this specimen the deviation in specimen responses was observed at an approximate load of 3 kips (Figure 77). From the load vs. cross-section depth (Figure 74), the cracking again appears to be on the lower side of the specimen, with both sides exhibiting a degree of non-linearity in the strain distribution similar to Pile 1. This specimen did not experience failure prior to reaching the limit of the test frame, but at the latter stages of loading, the steel on the lower right side of the specimen began to yield as is demonstrated by the strain increase observed in strain gauge 4 (Figure 76). For this specimen, no slip was observed at the locations of the interface gauges where maximum shear is expected, near the neutral axis.

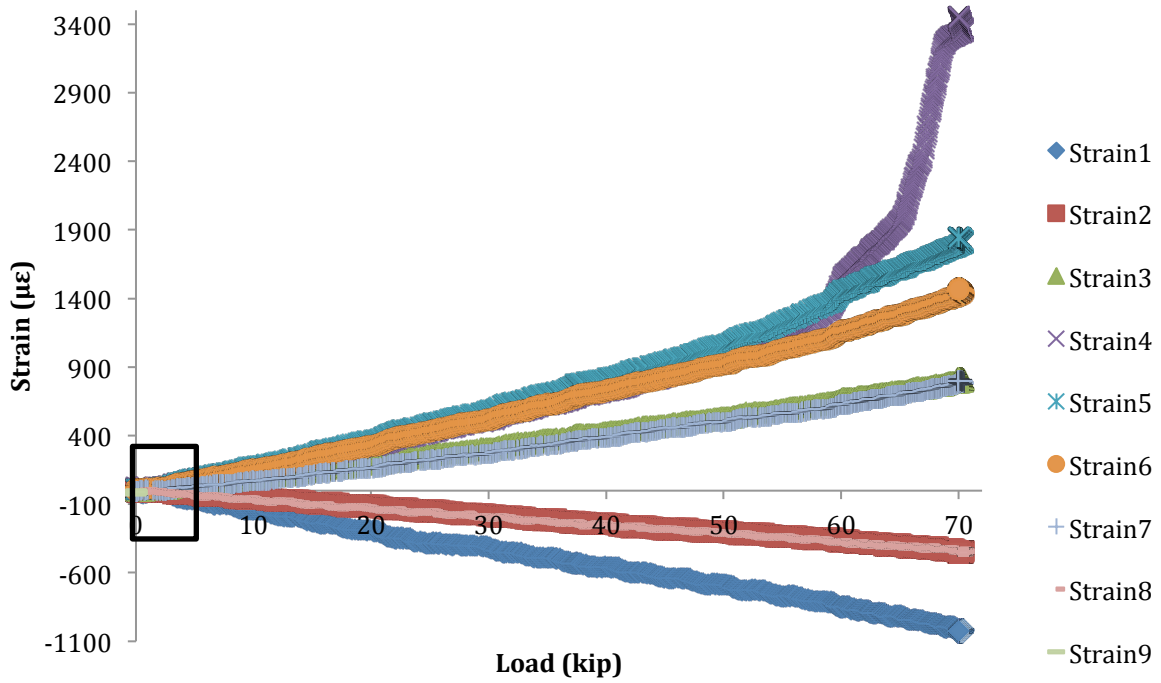


Figure 76 - Strain vs. load (all gauges) for (10-3/4" – 0.5" wall) – Pile 2 (full range of loading)

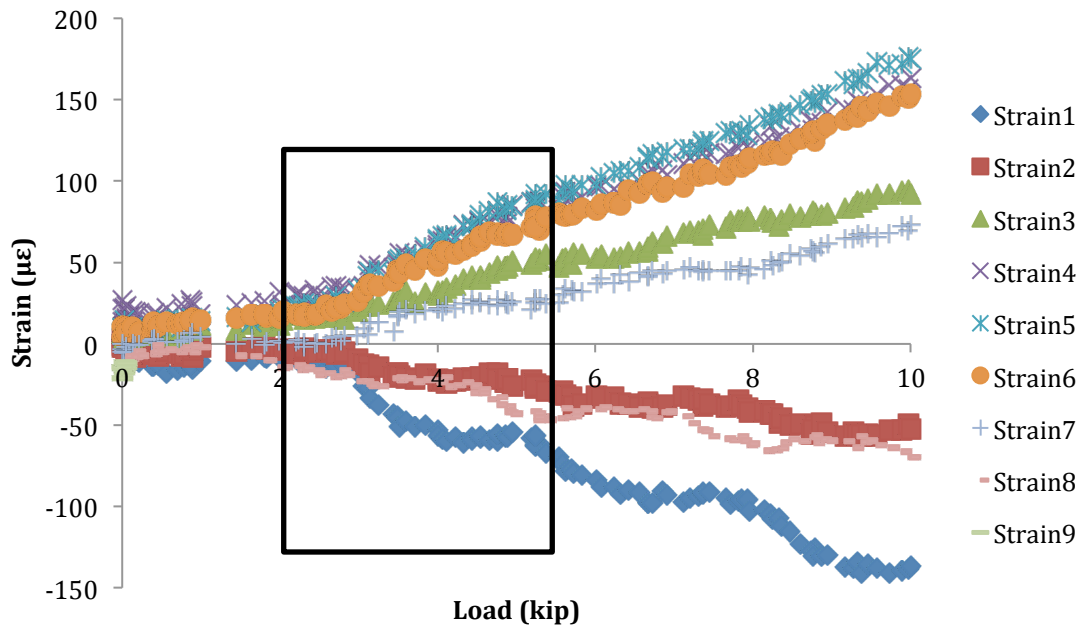


Figure 77 - Strain vs. load (all gauges) for (10-3/4" – 0.5" wall) – Pile 2 (partial range of loading)

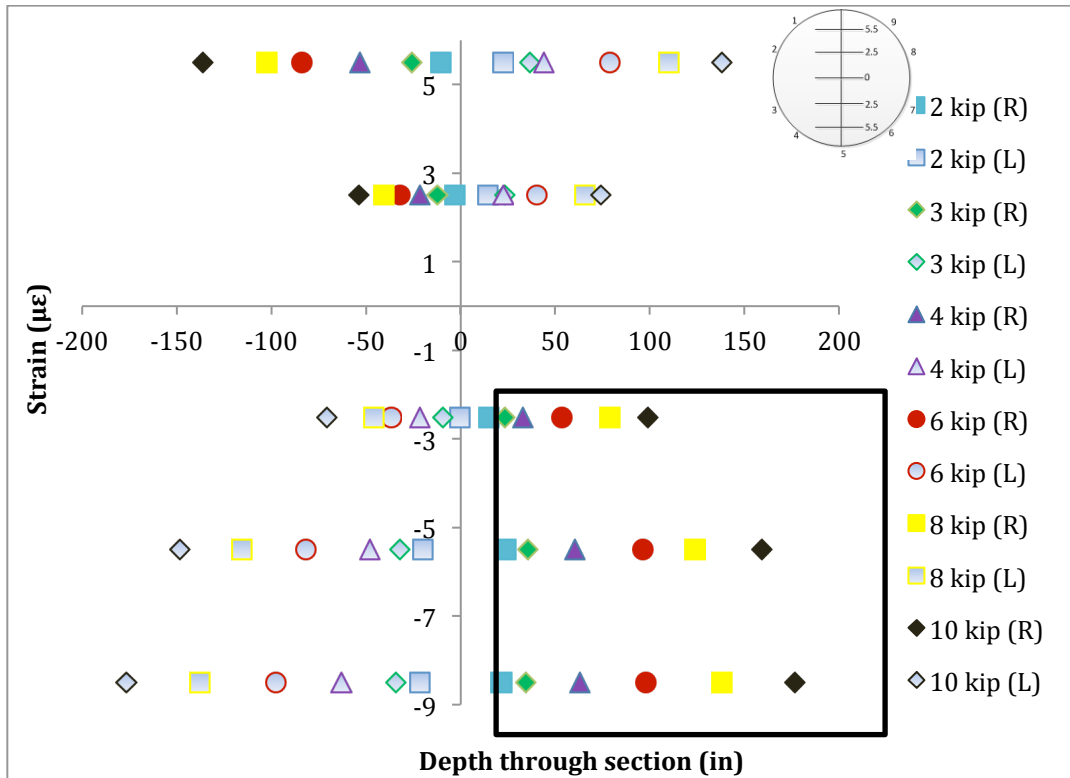


Figure 78 - Strain vs. load through cross-section depth (10-3/4" – 0.5" wall) – Pile 2

4.7 Summary of Analysis

Results from the compression testing scenarios (composite and core only), core section compression testing, flexural testing and push-through were presented in this section. Also included are the results from a finite element simulation of the compression testing.

While the compression tests of the stub sections were not taken to failure, the results from the experiments highlight the significant reserve capacity that exists over the design capacity. This reserve capacity was on the order of two to three times as much as the design capacity. While all of the specimens were loaded past the non-composite nominal capacity, only the loading on one specimen exceeded the composite nominal capacity; however all specimens exhibited the same general response suggesting that all would exceed the composite nominal capacity without failure.

Results from the compression tests from the cored sections at various depths demonstrated that there was an increase in compressive strength for the core concrete when compared to companion cylinder results. A visual inspection of the concrete throughout the pile at the locations of the cuts confirmed that good consolidation was achieved throughout the piles and no segregation was observed. This behavior suggests that the integrity of the concrete is not only maintained but is actually enhanced.

In the assessment of the bond performance, both results from the push-through testing and the flexural testing were considered. Results from the push-through testing indicated that the average shear bond strength is on the order of 0.291-0.525 ksi, which is in agreement with other bond strength results between steel and concrete. The flexural test results did not provide a direct measure of the bond strength, but demonstrated that the bond integrity is greater than the cracking strength of the composite section, as no slip was observed throughout the testing.

5 Findings and recommendations

5.1 Findings

The overall objective of the study was to evaluate the capacity of cast-in-place concrete filled tubular sections, which are commonly used as piles in the State of Wisconsin. A primary goal was to compare results from an experimental program to current design procedures and assess whether these procedures are appropriate for these members.

In this study, the structural capacity of cast-in-place steel tubular piling was investigated experimentally and numerically. For the experimental program, several full-length piles were partially driven and filled with concrete in the field to represent as near in-situ conditions as possible. These full-length piles were cut up into smaller testable sizes, which were also believed to be representative of the short braced lengths for piles driven into the ground. The smaller pile stub sections were run through a set of different tests, with a representative sampling taken from different depths of each pile for each test. The tests included compression tests on the entire stub cross-section, compression tests of the stub section where only the core was loaded, flexural tests of short pile sections, push-through tests, and testing of cored out samples from stub sections. In addition to the experimental program, a numerical study (finite element) was performed on the axially loaded sections to allow for extrapolation of the behavior of the piles to conditions more representative to in-service conditions.

5.1.1 Compression Behavior

The goal of the compression testing, which included tests on the composite section and a core only loading scenario, was to assess the axial capacity of the piles. With the piles typically being embedded in the ground, the restraint conditions were assumed to be fully braced along the pile length, as such stub sections (18" long) specimens were considered for the experimental program. For both loading scenarios, the capacity of the piles exceeded the capacity of the loading machine used for testing and as a result, no true measurements of ultimate capacity were achieved. This was

partially the result of the pile shells being thicker than planned and the piles having capacities greater than the upper design limit. Previous research on smaller tubular sections have indicated that this capacity is typically defined as a squash failure or local buckling phenomena, however neither was observed during testing. While no failures were observed in the test specimens, all specimens achieve greater capacities than the current nominal design capacities used by WisDOT (between 189-317% greater). All specimens were able to resist a total load of 1,000 kips without any observable failure mechanisms. For the 10-3/4" dia. (0.375" wall) specimen, this exceeded the design capacity allowed within the AASHTO LRFD Bridge Design Specification by about 3%. For the 10-3/4" dia. (0.5" wall) and 12-3/4" dia. (0.375" wall), this resistance is approximately 15% and 19% less than the AASHTO design capacity, respectively.

A series of finite element models were developed to simulate the behavior of the pile sections from both the experimental program and also extrapolate the behavior to in-service conditions. Some of the challenges that could not be accounted for in the model included the unbalanced loading resulting from slightly uneven cuts (and resulting uneven loading) of the stub sections and the complexity of welds within the stub sections. While the experimental program demonstrated that the pile sections remained within the elastic region, these geometric non-linearities could not be accounted for appropriately. As a result, the finite element simulation results were not able to match the experimental results for non-linear geometric scenarios; they did however match other results quite well. The finite element model was then expanded to assess the performance of pile sections embedded in soils representative of those within the State of Wisconsin. These expanded models assumed that soil resistance (similar in magnitude to non-composite pile capacity) would ultimately control the capacity of the pile design, but considered variations in soil stiffness parameters. The results from the model suggested that the influence of the soil is minimal on the capacity of the pile and that the pile basically behaves in a manner similar to the experimental sections, fully braced compression member.

In addition to the compression tests on the stub sections, cores were extracted from various depths along the pile for compression testing. Each section cored

provided a series of specimens for testing, but core breaks were common. It should be noted that the purpose of the core testing was to assess the compressive strength and consolidation of the internal concrete, which is typically allowed to free-fall within the pile during construction. Average compressive strength results from the core testing ranged from approximately 6,000 psi to 9,400 psi along the lengths of the piles tested. While these results are highly dependent on the strength of the concrete chosen by the contractor, these results (~7,600 psi average) were significantly higher than the compressive strength of companion cylinders tested (~4,700 psi). This trend suggests that the strength of core concrete is enhanced from the construction process. In addition to the compression test results, a visual inspection of cored sections and the ends of the cut sections indicated excellent consolidation with no apparent segregation of materials throughout the length of the pile.

5.1.2 Bond Behavior

The assessment of the bond performance was conducted using a series of push-through tests and flexural tests. The push-through tests were conducted on the stub sections to measure the shear bond capacity whereas the flexural testing was performed as an indirect measure of bond.

With the push-through testing, the cores of the stub sections were loaded until the core pushed through the steel shell. For the 10-3/4 in. diameter specimens, after the initial slip occurred, the resistance decreased as more load was applied and the remaining resistance was provided by the friction between the concrete and steel shell. For this scenario the shear stress to cause the initial slip was deemed the bond capacity. For the 10-3/4 in. diameter specimens, the average bond capacity ranged from 0.291 ksi to 0.525 ksi. For the 12-3/4" dia. specimens, a different phenomena was observed during testing in which after the initial slip, the specimens supported additional load. This behavior was attributed to an uneven internal surface at the location of the spiral seam welds, which provided mechanical resistance to the applied load which was overcome by crushing of the concrete at that location. For these specimens, the

average bond strength was 0.316 ksi, which is in the range of the 10-3/4 in. diameter specimens, but with significantly different behavior. While this stress is on the lower end of the bond strength of concrete to steel, shear stresses obtained from the finite element model at the interface for the composite section loading scenario were of a much smaller scale (0.011 – 0.024 ksi), indicating that the bond capacity will not be exceeded under the axial compression state of stress. It should also be noted that no interface separation was observed in the compression specimens either during or after testing.

In the flexural testing, short pile sections (11 ft.) were loaded laterally in a three point bending configuration to assess whether slip at the interface occurred under flexure. The specimens were subjected to concentrated axial loads at midspan with strain measurements taken around the perimeter of the member at the point of maximum flexure. The objective of the testing was to determine if interface slip occurred during the flexural loading. Of the four specimens tested, only one experienced a failure (10-3/4" dia. – 0.375" shell), which occurred due to a weld break. The 10-3/4" dia. (0.5" wall) specimens experienced yielding on the perimeter, whereas the two 12-3/4 in. diameter specimens reached the capacity of the test frame without failure or yielding. Throughout all of the flexural testing, cracking of the internal concrete occurred, but no slip was observed in any of the specimens.

5.2 Recommendations

In this investigation, the performance of cast-in-place concrete filled tubular piles was evaluated. Results from the investigation highlight the capacity of the tubular piles in compression and the interface bond between the concrete core and the steel shell.

Current practices in the State of Wisconsin design these pile sections primarily as axial compression concrete member by neglecting the contribution of the steel shell and limiting the allowable compressive strength of the concrete. This design approach is very conservative when compared to the capacity with the steel shell included. Based on the compression test results presented in this report, the contribution to the axial capacity provided by the steel shell is significant, and even more so when the composite section is considered. While none of the specimens were tested to failure (local

buckling), the test capacity of all specimens exceeds current design recommendations, indicating that the piles are being under-utilized. In addition, when considering the integrity of the bond, the results from the testing program indicate that the bond between the concrete core and the steel shell are similar to other composite sections. It should be noted that during the testing of the stub sections in compression and the short pile sections in flexure, there was no evidence of loss of bond. The bond evaluation required a fit-for-purpose test to ensure bond failure, a loading scenario that is not likely to occur under in-service conditions.

Clearly the final decision regarding the use of composite action is at the discretion of the Wisconsin Department of Transportation, but based on the results of the limiting testing program (limited in that all of the specimens tested did not exceed the AASHTO LRFD nominal capacity limits) it is reasonable to design for composite action due to the following considerations:

- The smallest pile tested (10-3/4" with 0.375" wall) was tested to beyond the AASHTO LRFD composite nominal capacity without any indications of failure. In fact, aside from some uneven loading effects, there was no indication of shell yielding or concrete crushing observed during the testing. While the other specimen sizes were not tested to this nominal design limit, no evidence of failure was observed either. The other specimens were tested to within 85% (10-3/4" w/ 1/2" wall) and 81% (12-3/4" w/ 3/8" wall) of the AASHTO LRFD nominal design capacities. At a minimum the Wisconsin Department of Transportation should be able to design to these values if a degree of conservativeness is necessary. This recommendation does not take into consideration the loss of integrity of the shell due to deterioration, unbraced lengths that produce column behavior that differs from that of a stub column, or low quality core concrete necessary for composite behavior.

While the research presented herein accomplished the primary objective of evaluating the structural performance of cast-in-place concrete filled tubular piles, the following recommendations for additional study should be considered:

- Compression testing of stub pile sections to failure to quantify the upper bound on the capacity. This task would allow for better characterization of the non-linear behavior of the pile at failure and aid in refining design procedures. Because none of the piles in this program were loaded to failure, the same piles could be reused for future work. This data would also allow for the expansion of a finite element model in the non-linear region with consideration of the soil-pile interaction behavior.
- Assessment of the strength gain phenomena observed with the concrete core material vs. companion specimens. The data gathered in this investigation has the potential to allow for more efficient designs by considering more slender sections.
- The numerical investigation demonstrated that the concrete strength had minimal effect on the behavior of the pile system in the elastic range. An evaluation of alternative core materials (e.g. light weight concrete, recycled concrete) in lieu of normal strength concrete may provide an economical benefit.
- Economic feasibility study on the cost-benefit of cast-in-place concrete filled tubular piles vs. comparable pile systems (e.g. H-piles, prestressed concrete piles).

6 References

- American Association of State Highway and Transportation Officials (AASHTO) (2010). AASHTO LRFD Bridge Design Specifications, American Association of State Highway and Transportation Officials. **5th Edition**.
- American Concrete Institute (ACI) (2008). Building Code Requirements for Structural Concrete (ACI 318-08) and Commentary. Farmington Hills, American Concrete Institute.
- American Institute of Steel Construction (AISC) (2005). Steel Construction Manual. Chicago, American Institute of Steel Construction.
- ASTM Standard C31 (2003). Standard Practice for Making and Curing Concrete Test Specimens in the Field. West Conshohocken, PA, ASTM International.
- Baig, M. N., J. Fan and J. Nie (2006). "Strength of Concrete Filled Steel Tubular Columns." Tsinghua Science & Technology **11**(6): 657-666.
- Choi, K. K. and Y. Xiao (2010). "Analytical Studies of Concrete-Filled Circular Steel Tubes under Axial Compression." Journal of Structural Engineering **136**(5): 565-573.
- Coduto, D. P. (2001). Foundation Design Principles and Practices, Prentice Hall.
- Fam, A., F. S. Qie and S. Rizkalla (2004). "Concrete-Filled Steel Tubes Subjected to Axial Compression and Lateral Cyclic Loads." Journal of Structural Engineering **130**(4): 631-640.
- Fujimoto, T., A. Mukai, I. Nishiyama and K. Sakino (2004). "Behavior of Eccentrically Loaded Concrete-Filled Steel Tubular Columns." Journal of Structural Engineering **130**(2): 203-212.
- Giakoumelis, G. and D. Lam (2004). "Axial capacity of circular concrete-filled tube columns." Journal of Constructional Steel Research **60**(7): 1049-1068.
- Gilbert, R., S. Najjar and Y. Choi (2005). Incorporating Lower-Bound Capacities into LRFD Codes for Pile Foundations. LRFD and Reliability Based Design for Deep Foundations, Austin, TX, ASCE.
- Google. (2011). "Google Maps." Retrieved June 6, 2011, from <http://maps.google.com/>.
- Gupta, P. K., S. M. Sarda and M. S. Kumar (2007). "Experimental and computational study of concrete filled steel tubular columns under axial loads." Journal of Constructional Steel Research **63**(2): 182-193.

- Harajli, M. (2004). "Comparison of Bond Strength of Steel Bars in Normal- and High-Strength Concrete." Journal of Materials in Civil Engineering **16**(4): 365-374.
- Hu, H.-T., C.-S. Huang, M.-H. Wu and Y.-M. Wu (2003). "Nonlinear Analysis of Axially Loaded Concrete-Filled Tube Columns with Confinement Effect." Journal of Structural Engineering **129**(10): 1322-1329.
- Johansson, M. and K. Gylltoft (2002). "Mechanical Behavior of Circular Steel--Concrete Composite Stub Columns." Journal of Structural Engineering **128**(8): 1073-1081.
- Jung, G. J., O. S. Kwon, S. J. Jung and M. M. Kim (2006). "Evaluation of full-sized cast-in-place pile capacity with artificial defects." Soil Mechanics 2006(1975): 10-20.
- Kim, D., A. V. D. Bica, R. Salgado, M. Prezzi and W. Lee (2009). "Load Testing of a Closed-Ended Pipe Pile Driven in Multilayered Soil." Journal of Geotechnical and Geoenvironmental Engineering **135**(4): 463-473.
- Lam, D. and K. Wong (2005). Axial Capacity of Concrete Filled Stainless Steel Columns. Design and Analysis, New York, NY, ASCE.
- Long, J. H., J. Hendrix and D. Jaromin (2009). Comparison of Five Different Methods for Determining Pile Bearing Capacities. Wisconsin Highway Research Program (WHRP). Madison, WI, Wisconsin Department of Transportation: 160 pp.
- Menzel, C. A. (1939). "Some Factors Influencing Results of Pull-Out Bond Tests." Journal of the American Concrete Institute 35: 516-543.
- O'Shea, M. D. and R. Q. Bridge (2000). "Design of Circular Thin-Walled Concrete Filled Steel Tubes." Journal of Structural Engineering **126**(11): 1295-1303.
- Olson, R. and T. Shantz (2004). Axial Load Capacity of Piles in California in Cohesionless Soils, Los Angeles, California, USA, ASCE.
- Roeder, C. W., B. Cameron and C. B. Brown (1999). "Composite Action in Concrete Filled Tubes." Journal of Structural Engineering **125**(5): 477-484.
- Sakino, K., H. Nakahara, S. Morino and I. Nishiyama (2004). "Behavior of Centrally Loaded Concrete-Filled Steel-Tube Short Columns." Journal of Structural Engineering **130**(2): 180-188.
- Schneider, S. (1998). "Axially Loaded Concrete-Filled Steel Tubes." Journal of Structural Engineering **124**(10): 1125-1138.
- Vable, M. (2002). Mechanics of Materials. New York, NY, Oxford University Press.

- Weathersby, J. H. (2003). Investigation of Bond Slip between Concrete and Steel Reinforcement Under Dynamic Loading Conditions. Ph.D. Dissertation, Louisiana State University.
- Wisconsin Department of Transportation (2005). Wisconsin Highway Construction Specifications, Wisconsin Department of Transportation.
- Wisconsin Department of Transportation (WisDOT) (2011). LRFD Bridge Manual, Wisconsin Department of Transportation.
- Wisconsin Geological and Natural History Survey. (2011). "Bedrock geology of Wisconsin." Retrieved June 28, 2011, from http://wisconsingeologicalsurvey.org/pdfs/pgszpdf/bedrock_geology.pdf.
- Wisconsin Geological and Natural History Survey. (2011). "Soil regions of Wisconsin." Retrieved June 28, 2011, from http://wisconsingeologicalsurvey.org/pdfs/pgszpdf/soil_regions.pdf.
- Wisconsin Geological and Natural History Survey. (2011). "Thickness of unconsolidated material in Wisconsin." Retrieved June 28, 2011, from http://wisconsingeologicalsurvey.org/pdfs/pgszpdf/thickness_unconsolidated.pdf.
- Xiao, Y., W. He and K.-k. Choi (2005). "Confined Concrete-Filled Tubular Columns." *Journal of Structural Engineering* **131**(3): 488-497.
- Yamamoto, T., J. Kawaguchi and S. Morino (2000). Experimental Study of Scale Effects on the Compressive Behavior of Short Concrete-Filled Steel Tube Columns, ASCE.

Appendix A – Chemical Testing Results of Steel Shells

06/19/01 TUE 08:03 FAX 17086147615

LALLY PIPE & TUBE

003



Spectrochemical Testing, Inc.
179 State Street • Struthers, Ohio 44471 • (330) 755-7373

June 6, 2001

Test Report:

Lally Pipe & Tube
514 Lowellville Rd.
Struthers, Ohio 44471

Phone (330) 750-1002
Fax (330) 750-1535

Attn. Mr. Jim Mocker

P.O. #1164 dated 6-4-01
(1) Steel pipe sample - 10 3/4" OD x .500" wall ERW - rec'd 6-5-01 for chemical and mechanical testing to meet ASTM A252 Grade 2 or 3.

Page 1 of 2

Results of Chemical Analysis: (ASTM E 415-99a)

Job # 27512

Lally 1164

ELEMENT

C	0.18
Mn	0.69
P	0.012
S	0.006
Si	0.01
Cu	0.01
Jim	0.003
Al	0.02
Cr	0.02
Mo	0.01
Ni	0.016
V	0.002
Co	0.002
Ti	0.002
Zr	0.002

Frank L. Galletta, Mgr.

RECEIVED JUN 08 2001



The results reported are limited to the sample tested and constitute data only with respect to the sample tested. Information and data in this report are correct and reliable to the best of our knowledge; however, results are not guaranteed and no responsibility is assumed. This report may not be reproduced except in full. Spectrochemical Testing, Inc. is accredited by the American Association for Laboratory Accreditation in the fields of Chemical and Mechanical Testing (Cert. #798.01 & 798.02).



Spectrochemical Testing, Inc.

171 State Street • Struthers, Ohio 44471 • (330) 755-7373

June 6, 2001

Test Report:

Lally Pipe & Tube
534 Lowellville Rd.
Struthers, Ohio 44471

Phone (330) 750-1002
Fax (330) 750-1535

Attn. Mr. Jim Mocker

P.O. #1164 dated 6-4-01
(1) Steel pipe sample - 10 3/4" OD x .500" wall ERW - rec'd 6-5-01 for chemical and mechanical testing to meet ASTM A252 Grade 2 or 3.

Page 2 of 2

Mechanical Test Results: (ASTM A 370-97a)

Job #	Sample #	Yield psi (EUL = 0.5%)	Tensile psi	Elong. / 2" %	Phos. %
27512	1164	57,500	73,000	40.0	0.012

* This material meets chemical and tensile requirements of ASTM A 252 Grade 3.

Franc L. Galletta
Franc L. Galletta, Mgr.

RECEIVED JUN 08 2001



This report is limited to the sample tested and constitutes data only with respect to the sample tested. Information and data in this report are correct and reliable to the best of our knowledge; however, results are not guaranteed and no responsibility is assumed. This report may not be reproduced except in full. Spectrochemical Testing, Inc. is accredited by the American Association for Laboratory Accreditation in the fields of Chemical and Mechanical Testing (Cert. #788.01 & 788.02).



178 State Street - Struthers, Ohio 44471 - (330) 756-7373

Feb. 12, 1999

Test Report

Lally Pipe & Tube
534 Lowellville Rd.
Struthers, OH 44471

Phone (330) 750-1002
Fax (330) 750-1535

Attn: Mr. James Mocker, Mgr.

P.O. #3705 dated 2-9-99

(1) steel pipe sample - 12 3/4" O.D. x .250" wall ERW - rec'd 2-11-99 for chemical and physical testing to meet ASTM A252 Grade 2 or 3.

Page 2 of 2

Mechanical Test Results: (ASTM E 8 - 95)

Spectro Job #	Lally #	Yield psi	Tensile psi	Elong. / 2" %	Phos. %
20923	3705	66,000	79,000	29.7	0.007

* Material meets chemical and tensile requirements of ASTM A 252 Grade 3.


Frank L. Galletta, Mgr.



05Jun03 14:51

TEST CERTIFICATE

No: PFB 4376

Sold By:

PRO-FAB

SKYLINE STEEL, LLC - PIPE GROUP

6726 PRESCOTT

ST LOUIS, MO 63147

Tel: 314-385-5477 Fax: 314 385-3538

P/O No 61459

Rel

S/O No PFB 102772-002

B/L No

Inv No

Shp

Inv

Sold To: (5)
SKYLINE STEEL LLC (IL)
18412 SOUTH WEST-CREEK DRIVE
TINLEY PARK, IL 60477

Ship To: (001)
PHEIFER BROTHERS CONSTRUCTION COMP
WI DOT PROJECT
DOUGLAS COUNTY
SUPERIOR, WISCONSIN

Tel: 708/444-0999 Fax: 708/444-0990

CERTIFICATE of ANALYSIS and TESTS

Cert. No: PFB 4376

05Jun03

Part No

10-3/4"OD SPIRALWELD PIPE A-252 GRADE 2 therM
.250 WALL X 40'

Pcs Wgt
77 86,363

Heat Number

Tag No

Pcs Wgt

C48356

2336A

20 22,432

C48486

2357A

17 19,067

C48489

2360A

19 21,310

C48489

2388A

21 23,554

Heat Number

*** Chemical Analysis ***

C48486

C=<.18> Mn=<.85> P=<.015> S=<.009> Si=<.012> TEN=<82500>
YLD=<66500> ELONG=<26.0>

C48489

C=<.17> Mn=<.88> P=<.011> S=<.006> Si=<.010> TEN=<79500>
YLD=<64000> ELONG=<29.0>

The undersigned hereby certifies that the above materials have been inspected and tested in accordance with the methods prescribed in the applicable specifications and results of such test shown above. In determining properties of characteristics for which no methods of inspection and testing are prescribed by said specifications the standard mill inspection and testing practices of this company have been applied. Unless specified otherwise in the results of such inspection and tests shown above, the undersigned believes that said materials conform to said specifications.

Melted and Manufactured in the U.S.A.

Name & Title

Subscribed and sworn to before me

This 5 day of June 2003

5183200 (REV. 02-04)

BETHLEHEM STEEL CORPORATION
 QUALITY ASSURANCE DEPARTMENT
REPORT OF TEST AND ANALYSIS

JOB CONTRACT NO.	PURCHASE ORDER DATE 10/16/01	PURCHASE ORDER NO. PAP-1423
SHIP TO BETHLEHEM STEEL CORPORATION ARROWS POINT PLANT ARROWS POINT, MARYLAND 21219	SHIPMENT NO. 41A-02395	MILL ORDER NO. 41134472A
	VEHICLE IDENTIFICATION	INVOICE NO. 41A-02395
		DATE SHIPPED 12/07/01

PA PIPE INC
 C/O SKYLINE STEEL, PIPE GROUP
 111 DENT DR NE
 CARTERSVILLE GA 30121

SHIP TO

PA PIPE INC
 1250 ST JOHNS RD
 CAMP HILL PA 17011

THICKNESS	TYPE	WIDTH	LENGTH
.346	M	22.00	

STEEL CHAR: HOT ROLLED OUTSIDE SLITTING & EDGE TRIM STRL Q DRY COILS-CE
 SPEC CODE: PA PIPE A252 GR3 45 KSI MIN YIELD 66 KSI MIN TENSILE ELONG 20% IN 2 FT

QUANTITY		Actual Weight	Coil/Lift Serial No.	Heat Number and/or Test Identification	Yield	Tensile Strength	ELONG		Bend
Pieces	Packages						In.	%	
1	1	21380	253480	411L9951					
1	1	21380	253480	411L9951	55,800	73,800	2	28.0	FRONT
				411L9951	58,900	74,100	2	33.0	FRONT

MELTED & MANUFACTURED IN THE USA

61089 Lead BCL 21206 - 7/23/02

Heat Number	CHEMICAL ANALYSIS			
	C	Mn	P	S
1L9951	.08	.92	.011	.012

I certify that the above results are a true and correct copy of actual results contained in records maintained by Bethlehem and are in full compliance with the requirements of the specification cited above. This test report cannot be altered and must be transmitted intact with any subsequent third party test reports, if required.

DEPARTMENT MANAGER
 QUALITY ASSURANCE

G. D. MARSH

DATE
 12/11/01 10:57
 PER

13Jul02 10:35

TEST CERTIFICATE

No: PAF 12566

Sold By:
PA PIPE, INC
SKYLINE STEEL CORP. - PIPE GROUP
1250 ST. JOHN'S ROAD
CAMP HILL, PA 17011
Tel: 717-737-9927 Fax: 717 975-7850

P20 No 41029
Pc1
S/O No PAF 2475-002
B/L No PAF 21206-001 Shp 23Jul02
Inv No

Sold To: (5)
SKYLINE STEEL CORPORATION (IL)
18412 SOUTH WEST-CREEK DRIVE
TINLEY PARK, IL 60477

Ship To: (001)
PHEIFER BROTHERS CONSTRUCTION
WI DOT PROJECT
WINNEBAGO COUNTY

Tel: 708/444-0999 Fax: 708/444-0950

CERTIFICATE of ANALYSIS and TESTS

Cert. No: PAF 12566
23Jul02

Part No
10-3/4"OD SPIRALWELD PIPE A-252 GRADE 2 Driam
365 WALL X 55'

Pcs 18
Wgt 40,068

Heat Number	Tag No	Pcs	Wgt
411L9961	C15872G	1	2,226
411L9961	C15872F	1	2,226
411L9961	C15872a	1	2,226
411L9961	C15874M	1	2,226
411L9961	C15874Q	1	2,226
411L9952	C15882L	1	2,226
411L9952	C15882Q	1	2,226
411L9952	C15882b	1	2,226
411L9952	C15882c	1	2,226
411L9951	C15884P	1	2,226
411L9951	C15884f	1	2,226
411L9951	C15884h	1	2,226
411L9951	C15892D	1	2,226
411L9951	C15892P	1	2,226
411L9952	C15958C	1	2,226
411L9952	C15958D	1	2,226
411L9952	C15958H	1	2,226

B-70 - 231 + 230
54800 + 01
These certs
copied + given to
Engineer 7/29/02

Heat Number	*** Chemical Analysis ***
411L9951	C=<.08> Mn=<.92> P=<.011> S=<.012> Si=<.017> TEN=<73,900> YLD=<56,700> ELONG=<34.0>
411L9952	C=<.08> Mn=<.92> P=<.011> S=<.012> TEN=<73,800> YLD=<55,800> ELONG=<28.0>
411L9961	C=<.07> Mn=<.92> P=<.012> S=<.014> TEN=<73,000> YLD=<55,700> ELONG=<30.0>

The undersigned hereby certifies that the above materials have been inspected and tested in accordance with the methods prescribed in the applicable specifications and results of such test shown above. In determining properties of characteristics for which no methods of inspection and testing are prescribed by said specifications the standard mill inspection and testing practices of this corporation have been

NOV. 29. 2001 4:54PM

BSC QA PRINT OFF SP TH MD

NO. 953 1. 2. 3

153200 (REV. 02-94)

BETHLEHEM STEEL CORPORATION QUALITY ASSURANCE DEPARTMENT REPORT OF TEST AND ANALYSIS

CONTRACT NO.	PURCHASE ORDER DATE 10/18/01	PURCHASE ORDER NO. PAIP-1423	INVOICE NO. 41A-02343
BETHLEHEM STEEL CORPORATION ARROWS POINT PLANT ARROWS POINT, MARYLAND 21219	SHIPMENT NO. 41A-02343	TRUCK ORDER NO. 41134472A	DATE SHIPPED 11/29/01
	VEHICLE IDENTIFICATION		

PA PIPE INC
C/O SKYLINE STEEL, PIPE GROUP
111 DENT DR NE
CARTERSVILLE GA 30121

SHIP TO
PA PIPE INC
1250 ST JOHNS RD
CAMP HILL PA 17011

THICKNESS .346 TYPE M WIDTH 22.00 LENGTH
STEEL CHAR: HOT ROLLED OUTSIDE SLITTING & EDGE TRIM STRL Q DRY COILS-CE
PEC CODE: PA PIPE A252 GR3 45 KSI MIN YIELD 66 KSI MIN TENSILE ELONG 20% IN 2 II

QUANTITY		Actual Weight	Coil/Lift Serial No.	Heat Number and/or Test Identification	Yield	Tensile Strength	ELONG		Bend
Pieces	Packages						In.	%	
1	1	21100	253482	411L9952					FRONT FRONT
1	1	21100	253482	411L9952	55,800	73,800	2	28.0	
				411L9952	58,900	74,100	2	33.0	

MELTED & MANUFACTURED IN THE USA

61089 - BCL 21206 - 7/23/02

Heat Number	CHEMICAL ANALYSIS							
	C	Mn	P	S				
411L9952	.008	.02	.011	.012				

I certify that the above results are a true and correct copy of actual results contained in records maintained by Bethlehem and are in full compliance with the requirements of the specification cited above.
This test report cannot be altered and must be transmitted intact with any subsequent third party test reports, if required.

DEPARTMENT MANAGER,
QUALITY ASSURANCE
G. D. MARSH

DATE
11/29/01 11:25
PCR



179 State Street • Struthers, Ohio 44471 • (330) 755-7373

December 17, 2007

Test Report:

Lally Pipe & Tube
534 Lowellville Rd.
Struthers, Ohio 44471

Phone (330) 750-1002
Fax (330) 750-1535

P.O. # 2908 dated 12-13-07

(1) Steel pipe sample – 10-3/4" O.D. x .365" wall ERW new secondary steel pipe – rec'd 12-17-07 from Lally Pipe & Tube, Covington, Ky. facility for mechanical and chemical testing.

Page 1 of 1

Mechanical Test Results: (ASTM A 370-07)

Job #	Sample #	Yield (0.2%) psi	Tensile psi	Elong. / 2" %
57100	2908	55,000	73,000	30.4

Results of Chemical Analysis: (ASTM E 415-99a)

Job#	57100
Lally	2908
ELEMENT	%
C	0.20
Mn	0.98
P	0.014
S	0.004
Si	0.17
Cu	0.06
Sn	0.006
Ni	0.03
Cr	0.05
Mo	0.02
Al	0.037
V	0.004
Cb	0.002
Ti	0.003
Zr	0.002

*Lele 9-00
SP*

Frank L. Galletta, Mgr.
Frank L. Galletta, Mgr.

RECEIVED DEC 20 2007



The results reported are limited to the sample tested and constitute data only with respect to the sample tested. Information and data in this report are correct and reliable to the best of our knowledge; however, results are not guaranteed and no responsibility is assumed. This report may not be reproduced except in full. Spectrochemical Testing, Inc. is accredited by the American Association for Laboratory Accreditation in the fields of Chemical and Mechanical Testing (Cert. #786.01 & 788.02).

Appendix B – Core Sample Test Data

Table 13 - Core sample test data

Pile Section	Core #	Cut Length (in)	Load (lbf)	Pressure (psi)	Comments
1 B	1	8-1/16	77,318	6,163	Approx. 5% of surface area has voids; total conical failure from bottom
1 B	2	7-5/8	67,558	5,399	Approx. 5% of surface area has voids; side sheer, bottom to top
1 B	3	8-1/16	81,066	6,461	Conical sheer throughout, total failure (exploded)
1 E	1	8	99,567	7,899	Shear Plane at 45d through middle
1 E	2	8	104,058	8,251	Shear Plane at approx. 30d from bottom to middle
1 E	3	6-11/16	101,179	8,025	Broke out of core short, cut on both ends until even; S.P same as previous
1 I	1	-	-	-	Broke Short
1 I	2	-	-	-	Broke Short
1 I	3	-	-	-	Broke Short
1 N	1	8	107,420	8,520	Conical shear throughout
1 N	2	8	114,048	9,033	Conical shear throughout
1 N	3	8	123,982	9,803	Conical shear throughout
1 Q	1	8-1/16	107,568	8,544	Total conical shear (exploded)

Pile Section	Core #	Cut Length (in)	Load (lbf)	Pressure (psi)	Comments
1 Q	2	8-1/16	84,854	6,754	Conical shear throughout
1 Q	3	8-1/8	95,277	7,559	Conical shear, bottom to middle, slight
2 D	1	8	118,510	9,367	Shear Plane vertical down middle
2 D	2	7-7/8	92,731	7,356	Slight aggregate breakage on one end (<1/4"); Conical shear throughout
2 Q	1	8-1/16	105,758	8,365	Total conical shear (exploded)
2 Q	2	8-1/8	96,196	7,553	Slight agg. Breakage at Top, <1/4"; conical shear, total failure (exploded)
2 Q	3	8	97,242	7,708	Total conical shear (exploded)
2 U	1	8-1/16	100,947	7,995	Slight agg. Breakage at Top, <1/4"; conical shear, total failure (exploded)
2 U	2	8	93,308	7,392	Slight agg. Breakage at Top, <1/4"; conical shear, total failure (exploded)
2 U	3	8-1/8	99,108	7,875	Total conical shear (exploded)
2 X	2	8	122,436	9,677	Conical shear plane, fractured in middle
2 X	1	8	115,731	9,176	Shear plane conical; complete failure (exploded)
3 F	1	7-13/16	99,540	7,905	Slight shear at top to middle; conical
3 F	2	8-1/16	102,552	8,144	Conical shear, more through middle (vertical)
3 F	3	8	103,752	8,245	Perfect conical shear

Pile Section	Core #	Cut Length (in)	Load (lbf)	Pressure (psi)	Comments
3 F	4	6-7/8	105,437	8,365	Broke short, cut to longest possible even length; bottom to middle shear
3 K	1	-	-	-	Broke Short
3 K	2	-	-	-	Broke Short
3 K	3	-	-	-	Broke Short
3 K	4	-	-	-	Broke Short
3P	1	-	-	-	Broke Short
3P	2	-	-	-	Broke Short
3P	3	-	-	-	Broke Short
3P	4	-	-	-	Broke Short
3 R	1	8	82,416	6,545	Conical shear top to middle
4 D	1	8	70,624	5,638	Approximately 5% of surface area has air voids
4 D	2	8	94,634	7,517	Shear Plane at 45d through middle
4 D	3	8	76,940	6,115	Conical shear bottom to middle
4 D	4	8	92,703	7,362	Conical shear throughout (hour glass shaped break)
4 G	1	8	82,710	6,569	Total conical failure (exploded)

Pile Section	Core #	Cut Length (in)	Load (lbf)	Pressure (psi)	Comments
4 G	2	8	84,903	6,742	Slight agg. Breakage on one end, <1/4"; surface voids on approx. 5% of surface; complete conical failure
4 G	3	8-1/8	76,748	6,121	Conical shear, top to middle
4 G	4	8-1/8	83,034	6,605	Conical shear, bottom to middle
4 Q	1	-	-	-	Broke Short
4 Q	2	-	-	-	Broke Short
4 Q	3	-	-	-	Broke Short
4 Q	4	-	-	-	Broke Short
4 U	1	8-1/16	74,749	5,966	Slight agg. Breakage on one end, <1/4"; surface voids on approx. 2% of surface; conical shear top to middle
4 U	2	8-1/8	104,161	8,263	Conical shear bottom to middle
4 U	3	8	89,710	7,130	Conical shear top to bottom
4 U	4	8-1/8	87,241	6,933	Slight conical shear bottom to middle - approx. 3" up, 1/2" in from edge
4 Y	1	8	111,625	8,764	Conical failure
4 Y	2	8-1/8	101,956	7,965	Conical failure
4 Y	4	8-1/8	100,121	7,857	Conical fracture, top to bottom